A comparison between water circulation and terrestrially-driven dissolved silica fluxes to the Mediterranean Sea traced using radium isotopes

Joseph Tamborski, Simon Bejannin, Jordi Garcia-Orellana, Marc Souhaut, Céline Charbonnier, Pierre Anschutz, Mireille Pujo-Pay, Pascal Conan, Olivier Crispi, Christophe Monnin, et al.

A comparison between water circulation and terrestrially-driven dissolved silica fluxes to the Mediterranean Sea traced using radium isotopes

Joseph Tamborski[a], Simon Bejannin[a], Jordi Garcia-Orellana[b,c], Marc Souhaut[a], Céline Charbonnier[d], Pierre Anschutz[d], Mireille Pujo-Pay[e], Pascal Conan[e], Olivier Crispi[e], Christophe Monnin[f], Thomas Stieglitz[g,h], Valentí Rodellas[g], Aladin Andrisoa[g], Christelle Claude[g], Pieter van Beek[a]*

[a]LEGOS, Laboratoire d'Etudes en Géophysique et Océanographie Spatiales (Université de Toulouse, CNES, CNRS, IRD, UPS), Observatoire Midi Pyrénées, 14 Ave Edouard Belin, 31400 Toulouse, France

[b]ICTA, Institut de Ciència i Tecnologia Ambientals, Universitat Autònoma de Barcelona, 08193 Bellaterra, Catalunya, Spain

[c]Departament de Física, Universitat Autònoma de Barcelona, 08193 Bellaterra, Catalunya, Spain

[d]EPOC, Environnements et Paléoenvironnements Océaniques et Continentaux, Université de Bordeaux, CNRS, UMR 5805, Talence, France

[e]LOMIC, Laboratoire d'Océanographie Microbienne, Observatoire Océanologique, Sorbonne Universités, CNRS, UPMC Univ Paris 06, UMR7621, 66650 Banyuls/Mer, France

[f]GET, Géosciences Environnement Toulouse (Université de Toulouse, CNRS, IRD, UPS), Observatoire Midi Pyrénées, 14 Ave Edouard Belin, 31400 Toulouse, France

[g]Aix-Marseille Université, CNRS, IRD, INRA, Coll France, CEREGE, Europôle de l'Arbois, BP80, 13545 Aix-en-Provence, France

[h]Centre for Tropical Water & Aquatic Ecosystem Research, James Cook University, Townsville QLD 4811, Australia

*Corresponding author: joseph.tamborski@legos.obs-mip.fr

Abstract

The recirculation of seawater through permeable coastal sediments is increasingly recognized as an important source of nutrients, including dissolved silica (DSi), to the coastal ocean. Here, we utilized a Ra isotope (^{223}Ra, $^{224}Ra_{ex}$, ^{228}Ra) mass balance to quantify DSi fluxes driven by water recirculation to a small shallow coastal lagoon (La Palme; French Mediterranean) during June 2016, as compared to karstic groundwater spring inputs. The DSi flux driven by lagoon water recirculation (derived from $^{224}Ra_{ex}$) was approximately one order of magnitude greater (1,930 ± 1,650 mol d^{-1}) than the DSi load of the karstic groundwater spring (250 ± 50 mol d^{-1}) and greater than molecular diffusion (970 ± 750 mol d^{-1}). Lagoon water recirculation was a negligible source of ^{228}Ra, indicating that recirculation-driven DSi inputs occur over a time-scale of days. Offshore transects were studied to quantify fluxes of marine-derived submarine groundwater discharge (SGD) from the permeable sandy coastline adjacent to the lagoon, into the Mediterranean Sea. Surface water transects revealed near-shore enrichments of Ra and DSi, attributed to wave-setup and water exchange through the permeable beach between the lagoon and the sea. Upscaling over the 9.5 km stretch of sandy beaches results in a marine SGD-driven DSi flux of 2.3 ± 1.3 *10^4 mol d^{-1}, similar in magnitude to the Têt river during November 2016 (3.3 ± 2.4 *10^4 mol d^{-1}), the largest river in the region. A positive relationship between DSi and $^{224}Ra_{ex}$ in lagoon water and seawater, but not ^{228}Ra, suggests that $^{224}Ra_{ex}$ and DSi enrichments are derived from a similar source, the sediment (i.e. lithogenic particle dissolution), operating on short time-scales. A marine SGD-driven DSi flux to the Gulf of Lions (3.8 ± 2.2 *10^5 mol d^{-1}) is likely continuous over time. The relatively constant DSi inputs from water recirculation for the shallow lagoons and beaches along the French Mediterranean Sea may sustain primary production in the coastal zone. In comparison, terrestrial

groundwater and rivers supply temporally variable nutrient (N, P, Si) inputs via changes in regional precipitation, runoff and aquifer storage.

Keywords: recirculation; submarine groundwater discharge, pore water exchange, radium isotopes, dissolved silica, Mediterranean Sea

1. Introduction

Dissolved silica (DSi) is a major nutrient which partly supports diatom primary productivity in coastal oceans (Tréguer & De La Rocha, 2013). There is increasing evidence that fluxes of DSi to the coastal ocean may be enhanced either by dissolution of biogenic particles within permeable coastal sediments (Anschutz et al,. 2009) or by dissolution of the permeable sediment itself in the presence of seawater (Ehlert et al., 2016). In either scenario, the primary mechanism behind DSi transport to the water column is from the advective movement of pore water across the sediment-water interface or from the coastal aquifer, broadly defined as submarine groundwater discharge (SGD), "regardless of fluid composition or driving force" (Burnett et al., 2003). In the absence of terrestrial (i.e. fresh) groundwater inputs, this process may be defined as water recirculation or marine SGD, which includes both large-scale and short-scale (sometimes referred as pore water exchange; PEX) recirculation processes (Burnett et al., 2003; Santos et al., 2012).

Pore waters obtain unique geochemical signatures in terms of carbon (Cyronak et al., 2014), nutrients (Berner, 1980; Slomp & Van Cappellen, 2004), trace metals (Beck et al., 2010; Trezzi et al., 2017) and natural radionuclides (Garcia-Orellana et al., 2013; Moore, 1996) within permeable coastal sediment (Moore, 1999). DSi enrichments in pore waters, which cannot be explained by simple binary mixing between seawater and groundwater, have been observed in various coastal water bodies throughout the world (Anschutz et al., 2016; Ehlert et al., 2016;

74 Kim et al., 2005; Ullman et al., 2003; Urquidi-Gaume et al., 2016; Weinstein et al., 2011). This
75 non-conservative DSi enrichment, combined with terrestrial inputs of DSi (rivers and
76 groundwater), may have a significant biogeochemical impact on the coastal ocean. For example,
77 SGD-driven DSi inputs were suggested to help maintain mixed-algal populations in a bay
78 surrounded by heavy industry (Lee et al., 2009) and have also lead to increased diatom
79 assemblages adjacent to coastal groundwater springs (Welti et al., 2015). SGD-driven nutrient
80 fluxes, including DSi, have been shown to impact primary production in a setting dominated by
81 diffuse SGD, while groundwater spring environments were more variable (Sugimoto et al., 2017;
82 Tovar-Sánchez et al., 2014). In karstic watersheds, DSi is generally enriched in terrestrial
83 groundwater and depleted in ocean waters, making DSi a useful tracer of terrestrial SGD,
84 particularly when combined with radium isotopes (El-Gamal et al., 2012; Garcia-Solsona et al.,
85 2010a; Garcia-Solsona et al., 2010b; Null et al., 2014).
86 Naturally occurring radium isotopes (^{223,224,226,228}Ra) have been widely used to estimate
87 volumetric water fluxes, as these tracers can spatially integrate different flow paths over large
88 areas (Swarzenski 2007). These radionuclides are enriched in pore water relative to surface
89 waters due to alpha recoil following production from the decay of their particle-associated Th
90 parent, and due to desorption from sediment solids via cation substitution and displacement in
91 high ionic strength solutions (Webster et al., 1995). Mass balances of Ra isotopes can be used to
92 quantify inputs of SGD in enclosed and semi-enclosed environments (Beck et al., 2007; Rodellas
93 et al., 2017). Shore-perpendicular surface water transects from the coast to the open sea are
94 commonly investigated to determine net exchange offshore, which in turn can be used to derive
95 SGD fluxes from long-lived ^{226}Ra and ^{228}Ra surface water gradients (Moore, 2000a). Short-lived
96 ^{223}Ra ($t_{1/2}$ = 11.4 d) and ^{224}Ra ($t_{1/2}$ = 3.66 d) can be used to trace short time-scale processes, while

97 longer-lived ^{226}Ra ($t_{1/2}$ = 1,600 y) and ^{228}Ra ($t_{1/2}$ = 5.75 y) may capture longer time-scale
98 discharge processes (Cai et al., 2014; Rodellas et al., 2017).
99 Total SGD-driven DSi inputs are comparable or higher than riverine inputs in the
100 Mediterranean Sea (Rodellas et al., 2015). There is little information to date in the Mediterranean
101 Sea comparing the flux of DSi from water recirculation or marine SGD, either via dissolution of
102 sediment or biogenic particles, to that of terrestrial groundwater and riverine inputs (Anschutz et
103 al., 2016). The Mediterranean Sea is, globally considered, an oligotrophic sea rich in oxygen and
104 deficient in nutrients such as silica, nitrogen and phosphorous; however, nutrient budget
105 calculations are based on non-synoptic and sometimes sparse data (Durrieu de Madron et al.,
106 2011). The release of DSi from lithogenic particle dissolution in the presence of seawater has
107 been experimentally (Anschutz et al., 2009; Morin et al., 2015; Techer et al., 2001) and
108 physically (Ehlert et al., 2016) observed, and has been invoked as a mechanism to explain the
109 DSi imbalance in the Mediterranean Sea (Jeandel & Oelkers, 2015). At a regional scale, the Gulf
110 of Lions (France) is a nutrient sink compared to other Mediterranean regions (Schroeder et al.,
111 2010). Major Mediterranean basin river fluxes over the last several decades have experienced an
112 increase in nitrogen and decrease in phosphorus loadings due to anthropogenic activity (Durrieu
113 de Madron et al., 2011), which has considerably modified the N:P stoichiometry (Ludwig et al.,
114 2009); however, information on nutrient inputs from water recirculation to coastal lagoons and
115 from marine SGD to the Gulf of Lions remain poorly known.
116 In this study, we utilize a Ra mass balance in a shallow coastal lagoon to assess the
117 relative importance of DSi inputs from a karstic groundwater spring compared to lagoon water
118 recirculation. In addition, we provide a first-order approximation of the marine SGD-driven DSi
119 flux (from wave-setup and water exchange across permeable sand barriers) to the Gulf of Lions,

as compared to riverine DSi inputs. The purpose of this study is to demonstrate the broad importance of water recirculation in conveying DSi to the coastal ocean on a local and regional scale, and its general biogeochemical impact.

2. Methodology

2.1 Site description

La Palme lagoon is a small, shallow lagoon located on the French Mediterranean coastline (**Figure 1**). Tides have a minor influence on La Palme lagoon, as the tidal range in this area of the Mediterranean Sea is approximately 20 – 30 cm. Water exchange between the lagoon and the sea is confined to a small inlet in the southeast corner of the lagoon, and can be seasonally opened from high-energy storm-events, which frequently occur during winter months. Stream inputs vary seasonally with the local hydrologic conditions, and typically cease flow during the summer. A karstic groundwater spring feeds into a former wash basin (lavoir), which discharges into the northern basin of the lagoon via a small-stream. Groundwater discharge from this spring (salinity 4 – 10) varies between 0.01 – 0.04 m^3 s^{-1} (Bejannin et al., 2017; Stieglitz et al., 2013), and has been shown to maintain brackish ecosystem functioning in the lagoon during the dry summer months (Stieglitz et al., 2013).

Previous estimates of lagoon water recirculation within La Palme lagoon vary from 0.29 – 2.1 m^3 s^{-1} during summer 2009, estimated from a ^{222}Rn, water and salt balance, where strong winds were hypothesized to drive recirculated water exchange (Stieglitz et al., 2013). Bejannin et al. (2017) estimated a predominantly recirculation-driven flux between 0.56 – 1.7 m^3 s^{-1} during July 2009, derived from a ^{223}Ra and $^{224}Ra_{ex}$ mass balance, while Rodellas et al. (2018) recently estimated ^{222}Rn and water balance-derived recirculation fluxes between 0.5 – 1.0 m^3 s^{-1} in the northern basin of the lagoon, between June 2016 – June 2017. The northern, intermediate and southern lagoon basins have limited water exchange due to long surface water residence times

144 (Bejannin et al., 2017) from constructed dikes and railways which impede surface exchange
145 between basins (**Figure 1**). The southern basin encompasses the area between the lagoon outlet
146 and the railway dike; the intermediate basin is defined as the area between the railway dike north
147 to the 0.4 m bathymetric contour (during June 2016), which separates the intermediate basin
148 from the northern basin (**Figure 1**).

149 Surficial sediments (upper 5 centimeters) vary in grain size throughout the lagoon; fine-
150 grained sediments (≤ 50 μm) dominate the deepest (≤ 1.3 m) section of the northern basin of the
151 lagoon while fine-to-coarse grained sands (~100 – 500 μm) make up the rest of the northern
152 basin (41 – 60 % of bottom-surface area). Fine-to-coarse grained sands (~100 – 500 μm)
153 dominate the shallower intermediate (≤ 0.6 m) and southern (≤ 0.4 m) lagoon basins (> 90% of
154 bottom-surface area) (IFREMER, 2003). The permeable shoreline from the lagoon outlet north
155 toward Port-la-Nouvelle (**Figure 1**) is made up of fine-to-coarse sands (~200 – 500 μm). There
156 are no river or stream inputs along this 9.5 km stretch of coastline.

157 ## 2.2 Field sampling

158 La Palme lagoon surface waters were sampled between 14 and 16 June 2016. Surface
159 water samples were collected throughout the lagoon (~20 L) via submersible or hand pumps into
160 triple-rinsed plastic cubitainers for Ra analysis; water depth was simultaneously measured with a
161 leveling rod (**Figure 1**). Salinity and pH were measured *in-situ* using a WTW probe (Multi
162 3430), for all surface samples. Additional samples were taken from the groundwater spring to
163 determine the karstic groundwater endmember, as well as two salt evaporation ponds and a
164 sewage outlet. The discharge of the groundwater spring was directly measured using a flow-
165 meter (Hydreka BFM 801) during September 2016. Pore water samples were taken from select
166 locations (PZ1, PZ2 and PZ3; **Figure 1**) in the lagoon during March 2016 and June 2016 using a

stainless-steel drive-point piezometer for Ra isotopes; nutrient samples were collected during June 2016 only. Pore waters were collected between 20 – 140 cm depth below the sediment surface; depending on the station, this corresponded to specific sample depths of 20, 30, 40, 50, 75, 100 and 140 cm. Small volumes of pore water (<0.5 L) were sampled for Ra isotopes to prevent mixing between different depth layers and with overlying lagoon waters.

A wide-diameter (22 cm) fine-grained sediment core (D_{10} ~50 μm) was collected in La Palme Lagoon during November 2016 to determine the diffusive flux of Ra from the sediment to the water column (**Figure 1**). Additional sediment cores (10 – 20 cm in length; 10 cm diameter) were collected in May and September 2017 to define the vertical distribution of DSi at the sediment-water interface, to assess the diffusive flux between the sediment and the water column. Three to five stations were sampled for each basin of the lagoon (**Figure 1**); DSi core sampling was carried out manually using 10-cm diameter PVC tubes. Sealed cores were immediately brought to the shore for pore water extraction. A sub-sample of each core interval (1 – 2 cm thick slices) was immediately sealed in a pre-weighed vial for further water content determination and porosity calculation. A second sub-sample was placed in a centrifuge vial (0.2 μm VIVASPIN20; Anschutz and Deborde, 2016) and pore waters were extracted by centrifugation at 4000 rpm for 20 min. Waters were stored at 4°C until DSi analysis.

Five surface water transects (~100 L for Ra isotopes) were sampled offshore of La Palme Lagoon, into the Mediterranean Sea, during November 2016 aboard the *R/V Nereis II* (**Figure 1**). These profiles extend from 0.2 – 8.0 km offshore and cover over 7 km of the 9.5 km sandy shoreline between the outlet of La Palme lagoon and Port-la-Nouvelle (**Figure 1**). Depth profiles of salinity and temperature were measured at each station using a calibrated CTD (Sea-Bird SBE 19 SeaCat). Coastal surface waters and shallow (0.5 m) beach pore waters (dug from boreholes)

were sampled directly adjacent to the shoreline during the cruise (two northern beach stations; **Figure 1**). Pore waters were sampled in June 2016 at the two southern endmember stations in a shore-perpendicular transect between the lagoon and sea (**Figure 1**), from the shoreline to < 60 m distance from the sea across the beach (n = 3 samples per transect).

2.3 Analytical methods

Mediterranean surface water, karstic groundwater, lagoon surface water and pore waters (taken from the drive-point piezometer) were immediately filtered in the field (using 0.45 µm cellulose acetate filters) and stored in 20 mL polyethylene vials at −20 °C until analysis for DSi, NO_3^-, NO_2^-, and PO_4^{3-}. In the laboratory, samples were analyzed by colorimetry on a Seal-Bran-Luebbe autoanalyzer AA3 HR (Aminot and Kérouel, 2007); analytical precision for DSi, NO_3^-, NO_2^- and PO_4^{3-} is ± 0.1 µM, 0.05 µM, 0.02 µM and 0.02 µM, respectively. Samples were diluted either 10x or 100x with deionized water and analyzed for Ba, Sr and Si via ICP-OES; analytical precision is ≤ 10% for all analytes. Lagoon water saturation states (log Q/K) were calculated in PHREEQC (Parkhurst and Appelo, 2013) using the THERMODDEM database (Blanc et al., 2012).

Dissolved Ra was quantitatively adsorbed onto MnO_2 coated acrylic fiber by passing the water through the fiber at a low flow rate (< 0.5 L min^{-1}); fibers were triple rinsed with Ra-free deionized water and partially dried in a compressed air stream (Sun & Torgersen, 1998). Short-lived ^{223}Ra and ^{224}Ra were counted using a radium delayed coincidence counting system (RaDeCC) (Moore & Arnold, 1996). ^{223}Ra was determined from a second count approximately 10 days after the first count; ^{228}Th was determined from a third count ~4 weeks after sample collection to determine supported ^{224}Ra activities that are used to determine excess ^{224}Ra (denoted $^{224}Ra_{ex}$). Samples were counted again ≥ 6 months after collection to determine the

initial ^{228}Ra activity (Moore, 2008). Detector efficiencies were determined using ^{232}Th and ^{227}Ac standards in secular equilibrium with their daughters. Analytical counting uncertainties were estimated by standard rules of error propagation and are reported with a 1σ confidence interval (Garcia-Solsona et al., 2008a).

The sediment core for Ra analysis was incubated following the methods of Beck et al. (2007). The core was incubated in the laboratory with lagoon water (of a known Ra activity) for various time intervals, after which the overlying water was extracted and replaced with new lagoon water (of a known Ra activity), to determine the sediment Ra flux driven by diffusion and bioirrigation (polychaetes found within the core). Suspended particle concentrations in the lagoon surface waters were measured in February 2017 (during high winds) via vacuum filtration using 0.45 μm pore space filters. Additions of fine-grained dry-sediment (sieved to grain size ≥ 0.45 μm, ≤ 50 μm; sampled next to PZ1; **Figure 1**) were added to 20 L of Ra-free lagoon water, shaken for 5 min, and measured following the methodology outlined above, to determine the Ra flux driven by desorption of re-suspended sediments (n = 6; Luek & Beck, 2014).

DSi diffusive fluxes were calculated using Fick's first law for the May and September 2017 cores. The molecular diffusion coefficient value (Schultz and Zabel, 2006) was corrected for *in-situ* temperature and porosity (Boudreau, 1996). Porosity was calculated from particle density and water content determined by the weight difference between wet and freeze-dried sediment, after sea salt correction. The density of particles was estimated at 2.65 g cm^{-3} (Berner, 1980), i.e. mean density of alumino-silicate and calcium carbonate minerals. Sediment from the southern basin (~200 – 250 μm) was incubated with *in-situ* lagoon water (**Figure 1**) in order to assess the kinetics of DSi enrichment in pore water through lithogenic particle dissolution, for two different water/particle ratios (Anschutz et al., 2009). In the first incubation, 7 g sand and 6

mL water were continuously stirred. The second experiment consisted of 2 g sand with 40 mL water. One mL of water was regularly sampled and replaced by 1 mL *in-situ* lagoon water over 16 days.

3. Results

3.1 La Palme Lagoon

Four distinct geochemical endmembers were observed in La Palme Lagoon: i) the karstic groundwater spring (salinity = 8.4 ± 0.7); ii) an evaporative, hyper-saline pore water (salinity > 38); iii) the salt evaporation ponds (salinity = 48 – 69) and iv) the open Mediterranean Sea (salinity ~38) (**Figure 2**; **Figure 3**). Lagoon surface waters were brackish in the northern basin (salinity = 33 ± 5), reflecting inputs from the karstic groundwater spring, with increasing salinity in the intermediate (salinity = 40 ± 2) and southern (salinity = 42 ± 3) basins, both of which were higher on average than the open Mediterranean Sea (38; **Table 1**). The karstic groundwater spring exhibited Ra activities of 11 ± 3 dpm $100L^{-1}$ for ^{223}Ra, 710 ± 80 dpm $100L^{-1}$ for $^{224}Ra_{ex}$ and 450 ± 30 dpm $100L^{-1}$for ^{228}Ra (n = 4). Over the course of six different sampling events, Bejannin et al. (2017) found ^{223}Ra, $^{224}Ra_{ex}$ and ^{228}Ra activities between 16 – 43 dpm $100L^{-1}$, 427 – 652 dpm $100L^{-1}$ and 84 – 237 dpm $100L^{-1}$, respectively, linked to the changing salinity of the spring. Mean Ra activities (± STD) were greatest for lagoon pore waters and exhibited strong vertical gradients, where deep samples (^{223}Ra = 400 ± 270 dpm $100L^{-1}$, $^{224}Ra_{ex}$ = 5,500 ± 3,900 dpm $100L^{-1}$, ^{228}Ra = 2,800 ± 1,900 dpm $100L^{-1}$; n = 7) were approximately 5 – 10 times greater than shallow samples (^{223}Ra = 70 ± 49 dpm $100L^{-1}$, $^{224}Ra_{ex}$ = 1,060 ± 740 dpm $100L^{-1}$, ^{228}Ra = 500 ± 450 dpm $100L^{-1}$; n = 5; **Table 1**). The salt evaporation ponds (^{223}Ra = 7 – 51 dpm $100L^{-1}$, $^{224}Ra_{ex}$ = 287 – 676 dpm $100L^{-1}$, ^{228}Ra = 362 – 1,090 dpm $100L^{-1}$) likely contributed little Ra to La Palme lagoon, based on the measured Ra concentration and salinity (**Figure 2**); we found no evidence of a connection between the salt ponds and the lagoon through visual inspection. There

was no evidence of a Ra isotope or nutrient (DSi, NO_3^-) source from samples taken adjacent to the sewage outlet during June 2016 (**Figure 1**; **Figure 3**).

Lagoon waters in the northern basin showed high activities of Ra isotopes derived from the groundwater spring, where Ra activities were elevated closest to the spring (**Figures 2 & 3**). In the intermediate and southern basins of the lagoon, ^{223}Ra and $^{224}Ra_{ex}$ activities increased with increasing salinity. Despite these general trends, there was observable spatial variability between the three Ra isotopes. Lagoon waters adjacent to the groundwater spring outlet were highest in $^{224}Ra_{ex}$ and ^{228}Ra. ^{223}Ra was greatest at the intersection between the intermediate and southern basins, while $^{224}Ra_{ex}$ activities were lowest in the intermediate basin. In contrast, ^{228}Ra activities were more uniform throughout the entire lagoon, but lowest in the southern basin, near the outlet to the Mediterranean Sea (**Figure 3**). Lagoon waters were near equilibrium with respect to barite in the northern and intermediate basins and under-saturated in the southern basin; all lagoon basins were under-saturated with respect to celestine (**Table 2**). In the northern basin, we observed lagoon water Ra activity distributions that reflected two-endmember linear mixing between the groundwater spring and higher salinity lagoon waters (**Figure 2**); thus, barite (and celestine) precipitation likely did not scavenge Ra and therefore did not impact the distribution of dissolved Ra.

The spatial distribution of dissolved silica (DSi) was similar to that of $^{224}Ra_{ex}$ (**Figure 3**, **Figure 4**), with higher concentrations adjacent to the groundwater spring outlet, lower concentrations in the intermediate basin and elevated concentrations (above seawater) in the southern basin. DSi was negatively correlated with salinity in the northern basin (p value < 0.001; $R^2 = 0.79$) and positively correlated with salinity in the intermediate (p value = 0.0346; $R^2 = 0.34$) and southern (p value = 0.001; $R^2 = 0.65$) basins. DSi was positively correlated with

283 $^{224}Ra_{ex}$ in the northern (p value < 0.001; R^2 = 0.90) and southern (p value = 0.0146; R^2 = 0.42)
284 basins (**Figure 5**). In the northern basin, DSi was positively correlated with ^{223}Ra (p value =
285 0.0021; R^2 = 0.49) and ^{228}Ra (p value = 0.0342; R^2 = 0.35), while there was no relationship
286 between DSi and ^{223}Ra or ^{228}Ra in the intermediate and southern basins (**Figure 5**). Quartz and
287 amorphous silica were under-saturated in the surface waters of the lagoon (**Table 2**).

288 ## 3.2 Offshore Transects

289 Surface water transects sampled offshore of La Palme lagoon during November 2016
290 (**Figure 1**) displayed elevated $^{223,224,228}Ra$ and DSi near the coastline that decreased with
291 increasing distance offshore (**Figure 6**). Pore waters sampled from shallow (0.5 m) beach pits
292 next to the shoreline were significantly enriched in ^{223}Ra (44 – 65 dpm $100L^{-1}$), $^{224}Ra_{ex}$ (1,030 –
293 1,730 dpm $100L^{-1}$), ^{228}Ra (58 – 62 dpm $100L^{-1}$) and DSi (5.8 – 24.2 µM); mean pore water
294 salinity (37.0 ± 0.5) was slightly lower than coastal Mediterranean seawater (n = 8). Short-lived
295 $^{224}Ra_{ex}$ was significantly correlated with DSi in surface water samples (**Figure 5**). There are no
296 external input sources (i.e. rivers or streams) along the 9.5 km investigated shoreline to cause the
297 observed geochemical gradients, aside from molecular diffusion from the sediment, such that
298 surface enrichments were likely derived from marine SGD (exchange between permeable sand
299 barriers and wave-setup). Assuming that advection is negligible and the system is in steady-state,
300 we estimated horizontal eddy diffusivity (K_h; Moore, 2000a) between 18 – 70 $m^2\ s^{-1}$ for ^{223}Ra
301 and 14 – 219 $m^2\ s^{-1}$ for $^{224}Ra_{ex}$, for the five-surface water transects (≥ 200 m offshore).

302 ## 3.3 Sediment: Diffusive Fluxes & Dissolution Experiments

303 Ra fluxes from fine-grained sediments (J_{Ra}) were estimated for each individual
304 incubation time point as:

305 $$J_{Ra} = \frac{(Ra_t - Ra_o) * V}{A * t} \quad (1)$$

306 Where Ra_t is the measured Ra activity at time t, Ra_o is the initial Ra activity of the overlying
307 water, V is the water volume overlying the core and A is the sediment core surface area. Burrow
308 structures were apparent on the sides of the core; therefore, we assume that the measured Ra flux
309 was supported by both molecular diffusion and bioirrigation. Mean (± SD) ^{223}Ra and ^{224}Ra fluxes
310 equal 3.6 ± 1.4 and 75 ± 50 dpm m^{-2} d^{-1}, respectively (n = 5). We use an average of the first two
311 incubation time points for ^{228}Ra, which have the lowest analytical uncertainties, with an assumed
312 uncertainty of 50% (15 ± 8 dpm m^{-2} d^{-1}). Mean (± SD) fine-grained sediment (grain size ≥ 0.45
313 μm, ≤ 50 μm) available for desorption was 0.24 ± 0.05 dpm g^{-1} sediment dry weight for ^{224}Ra
314 and 0.008 ± 0.007 dpm g^{-1} for ^{223}Ra (n = 6).

315 Lagoon pore waters showed gradients of DSi at the sediment-water interface during June
316 2016, May 2017 and September 2017. The concentration of DSi in sandy sediments was between
317 10 and 100 μM at 10 cm depth (**Figure 7**). In muddy sediments of the northern basin and in sites
318 with sea-grass in the southern basin, DSi concentrations reached 400 μM at the bottom of the
319 cores (~10 – 20 cm depth). Permeable sandy sediments have relatively low and constant DSi vs
320 depth concentrations, unlike DSi profiles from muddy sediments which exhibit strong vertical
321 DSi gradients. The small DSi concentration gradient in permeable sandy sediments suggests that
322 DSi concentrations are homogenized through advective flows. Mean (±SD) diffusive fluxes of
323 DSi to the water column in May and September 2017 were 56 ± 51 and 188 ± 173 μmol m^{-2} d^{-1},
324 respectively (n = 12), considering both muddy and sandy sediments. The hydrologic conditions
325 in September 2017 were close to those of June 2016, with low water level and high salinities in
326 the water column; therefore, we assume that the gradient of DSi in June 2016 was in the range of
327 what was measured in September 2017 (**Figure 7**). DSi fluxes were highest in the northern and

the southern basins. Accordingly, the total diffusive DSi flux, assessed from the addition of fluxes for each basin, equaled 970 ± 750 mol d^{-1} in September 2017 (**Table 3**).

The release of DSi from lithogenic particle (i.e. sediment) dissolution in the presence of lagoon water from the incubation experiments showed a constant increase in DSi of 100 µM for the first several days until a stable, saturated equilibrium concentration was reached (**Figure 8**). DSi increased with a slope of 82 µM d^{-1} in the experiment with a water/rock ratio (W/R) of 6 mL water/7 g sand. After 3 days DSi remained below 200 µM, close to the concentration at equilibrium with quartz. DSi increased for 10 days at a rate of 12 µM d^{-1} in the incubation with a higher W/R (40 mL water/2 g sand; **Figure 8**).

4. Discussion

4.1 Ra isotope distributions in La Palme lagoon

Ra isotope activity distributions in the lagoon waters are influenced by inputs from the groundwater spring and the lagoon bottom-sediments (**Figure 2**), in addition to decay and mixing. The mean $^{224}Ra_{ex}/^{223}Ra$ and $^{224}Ra_{ex}/^{228}Ra$ activity ratio of the groundwater spring was 84 ± 21 and 1.7 ± 0.3, respectively (**Figure 9**). Lagoon surface waters closest to the mouth of the groundwater spring have relatively high $^{224}Ra_{ex}/^{223}Ra$ and $^{224}Ra_{ex}/^{228}Ra$ activity ratios; the activity ratios quickly decreased with increasing distance away from the groundwater spring (distance from spring measured using current high-resolution imagery in Google Earth; assumed 10% uncertainty). $^{224}Ra_{ex}/^{223}Ra$ activity ratios of the lagoon waters reached a relatively constant value near the boundary between the northern and intermediate basins, reflective of either the underlying pore waters (~10 – 25; **Figure 9a**) or rapid mixing and homogenizing of surface waters between basins. At the interface between the northern and intermediate basin, there was a pulse in the $^{224}Ra_{ex}/^{228}Ra$ activity ratio, most likely reflecting inputs from pore water (**Figure 9b**). $^{224}Ra_{ex}/^{228}Ra$ activity ratios between the intermediate and southern basins began to increase

with increasing distance from the groundwater spring. This increase possibly reflects the changing grain-size of the surficial bottom sediments (less ^{228}Ra present due to smaller sediment surface-area of the larger grains), where the bottom-sediment transitioned from finer-grained sediment in the north to increasingly coarser-grained surficial sediment in the intermediate and southern basins (i.e. **Figure 7**), in addition to increased water recirculation likely as a consequence of higher sediment hydraulic conductivities. The bottom-sediment was clearly the source controlling the distribution of short-lived Ra isotopes in the overlying waters of La Palme lagoon, while the groundwater spring influenced the Ra distribution closest towards the groundwater spring outlet in the northern basin.

The apparent Ra age of the lagoon waters may be estimated using $^{224}Ra_{ex}/^{223}Ra$ and $^{224}Ra_{ex}/^{228}Ra$ activity ratios (Moore et al. 2006). The use of Ra activity ratios to derive apparent ages considers a principal source of Ra at a set activity ratio, which will decrease as a function of the distance from the input source due to radioactive decay and mixing (Moore et al., 2006). Surface water samples taken within several hundred meters of the karstic groundwater spring may be dated (Bejannin et al., 2017); however, the strong influence of pore waters and bottom-sediment prevents us from accurately using Ra activity ratios to estimate water ages between lagoon basins at the scales considered here (several km). Thus, we cannot combine the lagoon water age and the basin water volume to derive a surface water exchange rate between basins and with the sea.

4.2 Ra mass balance for La Palme lagoon: Estimation of water recirculation fluxes

A one-box mass balance is constructed to assess the inventory of dissolved Ra in La Palme lagoon during June 2016 (Equation 2),

$$J_{out} + J_{decay} = J_{spring} + J_{sediment} + J_{desorp} + J_{recirculation} \quad (2)$$

where J_{out} is the Ra water flux lost from the lagoon to the Mediterranean Sea, J_{decay} is the Ra lost from radioactive decay, J_{spring} is the brackish groundwater Ra input from the karstic groundwater spring in the northern basin, $J_{sediment}$ is the Ra input from the bottom sediments which includes both molecular diffusion and bioirrigation, J_{desorp} is the Ra input from desorption of re-suspended sediments and $J_{recirculation}$ is the Ra exchanged from water recirculation. Ra inputs from molecular diffusion and bioirrigation, determined from the sediment core incubation experiments, are explicitly separated from Ra inputs driven by lagoon water recirculation. Terms used in the mass balances are summarized in **Table 4**.

The groundwater spring Ra flux is estimated as the mean endmember Ra activity multiplied by the discharge of the groundwater spring (**Table 1**), which was manually measured at its outlet using a flow-meter in September 2016 (0.025 ± 0.005 m^3 s^{-1}). Here we assume that the flow of the groundwater spring was relatively constant during the dry season, between June and September. The small streams in the northern basin were not flowing during the June 2016 sampling campaign and therefore are not considered.

Ra isotopes released from re-suspended sediments were quantified following the methods of Luek and Beck (2014). The amount of ^{223}Ra and ^{224}Ra available for desorption (X_{desorp}) from fine-grained sediment (**Section 3.3**) equal 0.008 ± 0.007 dpm g^{-1} and 0.21 ± 0.05 dpm g^{-1} sediment dry weight, respectively, whereas desorption for ^{228}Ra and coarse-grained sediment is assumed to be negligible. A maximum suspended sediment concentration (C_{sed}; 40 ± 10 mg L^{-1}) measured during a high-wind event (max wind gust speed = 20 m s^{-1}; February 2017) is used to represent the maximum potential input of Ra desorbed from re-suspended sediments; we assume a maximum concentration of new sediments are re-suspended once per day. The Ra flux driven by the desorption of re-suspended sediment (J_{desorp}) was estimated with respect to the volume of

water within the lagoon (V), and represents the smallest input source of Ra by an order of magnitude. Ra inputs from molecular diffusion and bioirrigation are estimated using the results from the sediment incubation experiment, which contained visible burrow structures, indicative of bioirrigation (**Section 3.3**). For coarse-grained sediment, we assume that the Ra sediment fluxes are ~50% lower than the fine-grained sediment fluxes, as observed in coastal sediments from Long Island Sound (Garcia-Orellana et al., 2014). Diffusive fluxes are multiplied by the surface area of the lagoon with respect to the distribution of fine (~25%) and coarse-grained (~75%) surficial sediments. Experimental diffusive fluxes (**Table 4**) are in relative agreement with previous estimates for shallow water basins using the same technique, including Venice lagoon (^{223}Ra = 1.1 dpm m^{-2} d^{-1}; ^{224}Ra = 32 dpm m^{-2} d^{-1}; ^{228}Ra = 27 dpm m^{-2} d^{-1} in Garcia-Solsona et al., 2008b) and Jamaica Bay, NY (^{223}Ra = 1.1 dpm m^{-2} d^{-1}; ^{224}Ra = 28 dpm m^{-2} d^{-1}; in Beck et al., 2007).

During June 2016 the inlet between the lagoon and the Mediterranean Sea was only partially open, with visibly minor surface water exchange. Therefore, the mass balance is simplified by assuming that the net surface water exchange between the lagoon and the sea (J_{out}) was only significant in the area of the southern basin between the culvert and lagoon outlet (**Figure 1**), based on the observed surface water salinity distribution (~38; **Figure 3**). Surface water exchange farther north of this location is primarily restricted by constructed railway dikes (**Figure 1**). Ra surface water exchange fluxes are calculated by subtracting the coastal Mediterranean surface water Ra activity from the mean Ra activity in this section of the lagoon (^{223}Ra = 11.4 ± 3.5 dpm 100L^{-1}; ^{224}Ra$_{ex}$ = 197 ± 41 dpm 100L^{-1}; ^{228}Ra = 156 ± 52 dpm 100L^{-1}; n = 5), and are multiplied by the volume of lagoon water in this section (4.0 *10^{4} m^{3}), with an assumed flushing rate of 1.0 d (Stieglitz et al., 2013). The ^{228}Ra deficit from exchange with the

Mediterranean Sea is equal to 6.0 ± 2.0 *10^7 dpm d^{-1}, approximately in balance with the ^{228}Ra inputs from diffusion and bioirrigation (4.3 ± 3.0 *10^7 dpm d^{-1}) and the groundwater spring (1.0 ± 0.2 *10^7 dpm d^{-1}). The export flux of ^{223}Ra and $^{224}Ra_{ex}$ to the Mediterranean Sea is approximately 0.4 ± 0.1 *10^7 dpm d^{-1} and 7.4 ± 1.6 *10^7 dpm d^{-1}, respectively.

From the mass balance (Eq. 2), the $^{224}Ra_{ex}$ flux supplied by water recirculation is equal to 6.4 ± 1.9 *10^8 dpm d^{-1}; the ^{223}Ra flux is highly uncertain (4.4 ± 6.6 *10^6 dpm d^{-1}) and inputs of ^{228}Ra are negligible. Differences in Ra-derived water recirculation fluxes are interpreted to reflect the time-scale length of water recirculation through the lagoon sediment (Rodellas et al., 2017). The water recirculation flux drives significant inputs of $^{224}Ra_{ex}$ but not ^{228}Ra, suggesting that recirculation is operating on a time-scale of days. The $^{224}Ra_{ex}$ flux is divided by the average shallow pore water $^{224}Ra_{ex}$ activity (20 – 40 cm depth; **Table 1**) to estimate a volumetric water recirculation flux, assuming the $^{224}Ra_{ex}$ deficit is balanced by inputs of water recirculation through the lagoon sediment.

The volume flux of water recirculation to La Palme lagoon during June 2016 is 0.70 ± 0.51 m^3 s^{-1} for $^{224}Ra_{ex}$; uncertainties are propagated throughout each term in Equation 2. If the "true" $^{224}Ra_{ex}$ pore water endmember is from a shallower depth (< 20 cm), then the water recirculation flux will be larger (Cook et al., 2018). In comparison, Stieglitz et al. (2013) estimated a water flux between 0.4 – 2.1 m^3 s^{-1} during summer 2009 from a combined ^{222}Rn, water and salt balance, which was hypothesized to be driven by wind-forcing, while Bejannin et al. (2017) estimated a predominantly recirculation-driven flux between 0.56 – 1.7 m^3 s^{-1}. It is important to note the Ra mass balance calculations in Bejannin et al. (2017) used the karstic groundwater spring as the Ra endmember (opposed to pore water collected from permeable sediments), while the diffusive flux of Ra from the sediments was underestimated; further, the

study was conducted under different seasonal conditions (July 2009), in which the lagoon was completely closed off to the sea. As noted by Rodellas et al. (2018), water recirculation in the northern basin of La Palme lagoon varies over time. The $^{224}Ra_{ex}$-derived water recirculation flux (0.70 ± 0.51 m^3 s^{-1}), divided by the volume of water within the lagoon ($2.28 * 10^6$ m^3) during the time of sampling (**Table 4**), suggests that 2.6 % of the lagoon volume was recirculated through the sediment per day, in agreement with previous summer-time estimates (1.4 – 7.0 %; Stieglitz et al., 2013). The $^{224}Ra_{ex}$-derived water recirculation flux, normalized to the lagoon basin surface area (**Table 4**), is therefore 1.3 ± 1.0 cm d^{-1}. The physical mechanisms that may drive water recirculation through permeable sediments are summarized in Santos et al. (2012). Drivers such as density gradients (temperature and/or salinity), flow- and topography-induced advection, and shear-stress may recirculate water through the permeable sediment of La Palme lagoon. During the five days preceding the lagoon surface water sampling, mean wind speed was approximately 6.3 m s^{-1} with mean wind gusts of 16.0 m s^{-1} (www.weatherunderground.com); we speculate that wind may be an adequate driver of water recirculation in La Palme lagoon during this time period, as hypothesized by Stieglitz et al. (2013). Cook et al. (2018) found that pore water ^{222}Rn profiles in La Palme lagoon were consistent with wave action-driven recirculation, locally generated by winds.

4.3 DSi fluxes: terrestrial vs. marine sources

4.3.1 La Palme lagoon

There is an enrichment of DSi in the hyper-saline (> 38) lagoon waters of the intermediate and southern basins, which cannot be explained by external inputs (e.g. salt ponds, offshore Mediterranean seawater; **Figure 3F**, **Figure 4**, **Figure 5**). Intermediate and southern basin surface waters increased in DSi with increasing salinity, reflecting underlying pore waters. DSi may be added to overlying lagoon waters from bottom-sediments through both molecular

diffusion and water recirculation; in addition, DSi in lagoon waters can be concentrated by evaporation, which we do not quantitatively take into account here. In La Palme lagoon, the DSi enrichment is not likely associated with biogenic Si dissolution (Loucaides et al., 2008), as bottom sediments in the intermediate and southern basins are dominated by fine-sand (**Figure 7**). A similar result was concluded in a sandy barrier island subterranean estuary, where diatom dissolution within the sediment was unable to support enriched DSi concentrations in pore waters, which was primarily driven by sediment dissolution from seawater recirculation (Ehlert et al., 2016). Longer recirculated water residence times permit a longer contact period of pore fluid with sediment, which in turn increases pore water DSi concentrations via lithogenic particle dissolution, until a saturated equilibrium concentration is reached (**Figure 8**).

Experimental sediment dissolution rates conducted with sandy La Palme lagoon sediment (from the southern basin; ~200 – 250 μm) showed very high dissolution rates with the two-different water/rock ratios tested (82 and 12 μM DSi d^{-1}; **Figure 8**). These values are much higher than previously reported rates of 1.18 μM DSi d^{-1} for 50 g of sediment (170 μm grain size) in 27 mL seawater (Ehlert et al., 2016) and of 0.23 μM DSi d^{-1} for 50 g of sediment (300 μm grain size) in 50 mL seawater (Anschutz et al., 2009). From the $^{224}Ra_{ex}$ mass balance, 1.3 ± 1.0 cm d^{-1} of lagoon water is recirculated through the bottom-sediment; this relatively low rate of pore water advection is in agreement with the relatively low concentration of pore water DSi in sandy sediments (**Figure 7**), despite the high rate of DSi dissolution obtained experimentally (**Figure 8**).

Pore water DSi is high only in sediment with high porosity, i.e. muddy and low permeable sediments, where recirculation is likely restricted (**Figure 7**). In sandy permeable sediments (porosity below 50%), pore waters of the top cm below the sediment-water interface

491 have mean DSi concentrations below 100 μM, suggesting that the residence time of pore waters
492 is between 1 and 8 days (**Figure 8**). The DSi flux driven by water recirculation is estimated as
493 the mean concentration difference between the shallow pore water within the top 10 cm of sandy
494 sediments and the lagoon water overlying the sediment. We do not observe significant seasonal
495 variability in the shallow pore water DSi endmember concentration (**Figure 7**); therefore, we
496 take a mean pore water DSi concentration equal to 32 ± 14 μM (n = 17) from June 2016, May
497 2017 and September 2017 (0 – 10 cm depth). The mean DSi endmember concentration is
498 multiplied by the $^{224}Ra_{ex}$-derived recirculated water flux (0.7 ± 0.5 m^3 s^{-1}) to derive a DSi flux
499 equal to 1,930 ± 1,650 mol d^{-1} (0.42 ± 0.36 mmol m^{-2} d^{-1} over the entire lagoon), at least a factor
500 of two greater than inputs from molecular diffusion alone (**Table 5**). If the "true" Ra endmember
501 is from a shallower depth (< 20 cm; Cook et al., 2018), then the water recirculation flux will be
502 larger; this would effectively increase the DSi flux driven by water recirculation, and therefore
503 the flux calculated above is a conservative estimate. The significant relationship between short-
504 lived $^{224}Ra_{ex}$ and DSi, but not with ^{228}Ra, indicates that the water recirculation-driven DSi flux
505 operates over a time-scale of days. ^{224}Ra is regenerated daily in the sediment from its longer-
506 lived (surface-bound) parent ^{228}Th, such that continuous recirculation inputs can be easily traced.
507 Longer-term studies in La Palme lagoon indicate significant water recirculation in the northern
508 basin, between 0.5 – 1.0 m^3 s^{-1} regardless of the season (Rodellas et al., 2018), signifying that
509 various forcing mechanisms (wind, waves, density-gradients) continuously drive lagoon water
510 recirculation and therefore supply DSi to La Palme lagoon. The groundwater spring is enriched
511 in DSi, with a mean concentration of 114 ± 0.2 μM (**Figure 4**) and a resultant DSi flux equal to
512 250 ± 50 mol d^{-1} (**Table 5**). The sediment contribution of DSi through water recirculation (and
513 molecular diffusion) is an order of magnitude greater than the DSi flux from the groundwater

514 spring, indicating that water recirculation through the lagoon sediment is significant in
515 controlling the DSi inventory within La Palme lagoon.

516 ### 4.3.2 Offshore transects

517 On the seaward side of the lagoon, wind and wave action drive seawater into the sandy,
518 permeable beach face. Additionally, a hydraulic gradient exists between the lagoon and the sea
519 when lagoon water levels are high, driving lagoon water through the beach toward the sea; this
520 gradient may cease or reverse direction when lagoon water levels are low or when wind blows
521 from the sea towards the beach. We will broadly define flow paths which enter the
522 Mediterranean Sea from these two separate processes as marine SGD (Burnett et al., 2003);
523 being synonymous with the term "water recirculation" used for La Palme lagoon (Section 4.2).
524 Shallow pore waters sampled between the lagoon and sea were slightly reduced in salinity (37.0
525 ± 0.5; n = 8) compared to Mediterranean seawater; therefore, these samples likely reflect a
526 combination of a wave-setup endmember and an endmember driven by the hydraulic gradient
527 between the lagoon and sea, as traced by elevated ^{228}Ra activities (**Figure 6**).

528 Pore water can become enriched in DSi from lithogenic particle dissolution, depending
529 on the subsurface residence time (**Figure 8**). The DSi inventory of coastal surface waters
530 represents inputs from molecular diffusion (e.g. **Table 3**), bioturbation, lateral/onshore
531 advection, upwelling and marine SGD. We explicitly subtract coastal surface water DSi
532 concentrations from the shallow pore water samples collected along the beach to derive a non-
533 conservative DSi enrichment; this non-conservative DSi enrichment must be derived from
534 lithogenic particle dissolution from both wave-setup and exchange between the permeable sand
535 barrier. Beach pore water DSi concentrations were enriched over seawater concentrations (1.6 ±
536 0.1 μM, n = 36, ≥ 100 m offshore), with an average non-conservative pore water DSi enrichment

of 18 ± 7 µM during June and November 2016 (n = 8), after correcting for seawater. The observed Ra and DSi surface water enrichments must be driven by marine SGD inputs, as there are no other solute sources in this area to drive the observed gradients, aside from the partially open outlet of La Palme lagoon, adjacent to transect N4 (**Figure 1**).

^{223}Ra-derived horizontal eddy diffusivity was slightly lower than estimates derived from $^{224}Ra_{ex}$ (**Section 3.2**). $^{224}Ra_{ex}$, with respect to ^{223}Ra, is typically less sensitive to onshore advection of Ra-depleted offshore waters and the advection of Ra in the longshore direction, due to the shorter half-life of ^{224}Ra (Colbert and Hammond, 2007). We therefore use $^{224}Ra_{ex}$-derived horizontal eddy diffusivity in the ensuing analysis. Multiplying the ^{228}Ra surface water gradients (transects N1, N2 and N3 ≥ 200 m offshore; **Figure 6**) and the $^{224}Ra_{ex}$-derived horizontal eddy diffusivity, integrated over a 2.5 m thick impacted water column and distributed over the 9.5 km long shoreline, results in a ^{228}Ra flux driven by marine SGD between 3.7 – 13.5 $*10^8$ dpm d^{-1} for the three transects. Transect N4 is not included here, as it may be influenced by surface water exchange from the outlet of La Palme lagoon (**Figure 1**); ^{228}Ra uncertainties for transect N5 are relatively high and is therefore excluded from this analysis. Dividing the ^{228}Ra flux by the mean shallow beach pore water ^{228}Ra endmember (60 dpm $100L^{-1}$) results in a marine SGD flux between 0.6 – 2.2 $*10^6$ m^3 d^{-1}. Multiplying the marine SGD flux by the shallow beach pore water DSi enrichment (18 ± 7 µM) yields a DSi flux of 2.3 ± 1.3 $*10^4$ mol d^{-1} (2.4 ± 1.4 mol d^{-1} m^{-1} of shoreline). The ^{228}Ra marine SGD-derived DSi flux here is within the range of the DSi flux driven by brackish SGD to the entire Mediterranean Sea, between 1 – 28 mol d^{-1} m^{-1} of shoreline (Rodellas et al., 2015).

To assess the relevance of marine SGD-driven DSi fluxes, we will compare with DSi inputs from the largest river in the region, the Têt river (Sadaoui et al. 2016). The marine SGD

flux calculated above (0.6 – 2.2 *10^6 m^3 d^{-1}) is significantly higher than the discharge of the Têt river during November 2016 (2.69 ± 1.86 *10^5 m^3 d^{-1}). The DSi flux from the Têt river is calculated from the monthly mean discharge of the river gauging station (Station Y0474030; hydro.eaufrance.fr) and the mean DSi concentration of the river (Station 06172100; sierm.eaurmc.fr). Riverine DSi samples are not available after 2013; therefore, we take an average DSi concentration of 122 ± 25 μM (n=48) from January 2010 – December 2013. The amount of DSi supplied by the Têt river during November 2016 is estimated as 3.3 ± 2.4 *10^4 mol d^{-1}; therefore, the marine SGD-driven DSi flux is on the same order of magnitude as the DSi flux from the Têt river during November 2016 (**Table 5**). The Têt river varies in response to regional precipitation; the average monthly discharge for 2016 was 3.1 ± 1.6 *10^5 m^3 d^{-1} with a maximum during May (7.3 ± 6.3 *10^5 m^3 d^{-1}; DSi flux = 9.0 ± 2.9 *10^4 mol d^{-1}). The relative significance of marine SGD in supplying DSi to the coastal Mediterranean Sea is thus seasonally dependent with respect to the terrestrial DSi load supplied by coastal rivers and terrestrial groundwater.

Coastal lagoons and sandy beaches dominate the French Mediterranean coastline, from Perpignan to Montpellier, buffered on each end by impermeable rock. The shoreline length of sandy beaches within this region is approximately 160 km (**Figure 1**). If we assume that the marine SGD flux measured here, driven by wave-setup and water level differences between permeable sand barriers, affects the 160 km long shoreline in a similar manner, and that the derived $^{224}Ra_{ex}$, ^{228}Ra and DSi gradients offshore of La Palme lagoon are similar between each of these sandy beaches, then we may be able to provide a first-order approximation of the marine SGD-driven DSi flux to the sandy shoreline of the Gulf of Lions. Extrapolation of the DSi flux of 2.4 ± 1.4 mol DSi d^{-1} m^{-1} of shoreline for La Palme, over the 160 km sandy shoreline of the

583 Gulf of Lions, results in a marine SGD-driven DSi flux of 3.8 ± 2.2 *10^5 mol d^{-1}. This DSi flux
584 is between one and two orders of magnitude lower than the Rhône River (~2 *10^7 mol DSi d^{-1};
585 depending on the season), the largest river which discharges into the Gulf of Lions and the
586 Mediterranean Sea (Billen and Garnier, 2007; Ludwig et al., 2009). In contrast, Rodellas et al.
587 (2015) showed that total SGD-driven DSi inputs (terrestrial + marine flow paths) to the
588 Mediterranean can be comparable or higher than riverine inputs. Differences between the marine
589 SGD-driven DSi flux estimated here to the DSi flux supplied by the Rhône River is likely a
590 function of scale-length (only 160 km shoreline length) and the fact that the Rhône River is the
591 largest river in the Mediterranean Sea. The relative role of marine SGD as a source of DSi is
592 likely more significant in Mediterranean coastal areas which receive limited riverine inputs
593 (Trezzi et al., 2016).

594 ### 4.4 Potential nutrient limitation

595 The relationship between short-lived $^{224}Ra_{ex}$ and DSi for La Palme lagoon and the coastal
596 Mediterranean Sea (**Figure 5**) suggests that these dissolved constituents are derived from a
597 similar source, the sediment (**Figure 8**), operating over a time-scale of days. The constant wind
598 and wave action along the permeable shoreline of the investigated study area provides a
599 mechanism in which sediment is consistently exposed to seawater (or lagoon water), and
600 therefore, by this process, carries a distinct geochemical signature upon discharge back into the
601 sea or lagoon. A water recirculation-driven DSi flux derived from lithogenic particle dissolution
602 is likely a continuous DSi source over long time-scales, aside from minor variations in
603 recirculated water residence times within the permeable coastal sediment, as for example, due to
604 seasonally variable winds and storms. The relatively constant DSi inputs from water
605 recirculation for the shallow lagoons along the French Mediterranean Sea may sustain primary
606 production in the coastal zone. In comparison, terrestrial groundwater and rivers supply

607 temporally variable nutrient (N, P, Si) inputs via changes in regional precipitation, runoff and
608 aquifer storage (Michael et al., 2005; Slomp & Van Cappellen, 2004). For example, Rodellas et
609 al. (2018) estimated karstic groundwater discharge to La Palme lagoon during November 2016
610 that was approximately one order of magnitude higher than June 2016; such temporal variability
611 drives temporally variable nutrient loads that may impact primary production.

612 Analysis of La Palme lagoon water, Mediterranean seawater and pore water nutrient
613 ratios (DSi:DIN, DSi:DIP, DIN:DIP) reveals stark differences in the potential limiting nutrient of
614 La Palme lagoon and the coastal Mediterranean Sea (Garcia-Solsona et al., 2010b; Justic et al.,
615 1995). Here, DIN is equal to the sum of NO_3^-, NO_2^- and NH_4^+; DIP is equal to PO_4^{3-}. Surface
616 waters from the coastal Mediterranean Sea were limited in DIP (**Figure 10**), similar to other
617 karstic areas impacted by SGD along the Mediterranean Sea (Garcia-Solsona et al., 2010a;
618 Garcia-Solsona et al., 2010b) and the eastern Mediterranean basin (Krom et al., 2010).
619 Considering a mean beach pore water concentration of 0.18 ± 0.07 μM DIP (after subtracting
620 surface seawater concentrations; n = 8), the marine SGD-driven DIP flux (derived from the ^{228}Ra
621 surface water gradient calculations; Section 4.3.2) to the Mediterranean Sea is 0.02 ± 0.01 mol d^{-1}
622 ^{1} m^{-1} of shoreline (230 ± 130 mol DIP d^{-1} over the 9.5 km long shoreline), which is
623 approximately 5 – 23 % of the DIP load from the Têt river (~1 – 5 *10^3 mol P d^{-1}). In
624 comparison, the marine SGD-driven NO_3^- flux to the Mediterranean Sea is 5.7 ± 3.2 mol d^{-1} m^{-1}
625 of shoreline (5.4 ± 3.0 *10^4 mol N d^{-1}), considering a mean beach pore water concentration of 43
626 ± 28 μM NO_3^- (after subtracting surface seawater concentrations; n = 8). Therefore, marine SGD
627 along the Mediterranean shoreline drives a DIN:DSi flux ratio of approximately 2.4, higher than
628 Redfield ratio (0.8). This flux is at least a factor of two times greater than the NO_3^- load of the
629 Têt river (~1 – 3 *10^4 mol N d^{-1}).

La Palme lagoon surface waters were primarily DIN limited, with the exception of three samples taken closest to the karstic groundwater spring, which were limited in DIP (**Figure 10**). The NO_3^- load of the groundwater spring to La Palme lagoon during June 2016 (220 mol N d^{-1}; Rodellas et al., 2018) is likely the primary driver limiting nutrient utilization in the northern-most section of the lagoon (**Figure 3e**), in addition to DIN inputs (in the form of NH_4^+) from lagoon water recirculation (1,900 ± 900 mol N d^{-1} during June 2016). In comparison, the recirculation-driven DIP flux estimated for June 2016 was relatively minor (71 ± 36 mol DIP d^{-1}; Rodellas et al., 2018). The water recirculation-driven DIN:DSi flux ratio to La Palme lagoon is approximately 0.98 (1,900 mol DIN/1,930 mol DSi), slightly higher than Redfield ratio (0.8). An increase in recirculation-driven DSi inputs by lithogenic particle dissolution may not impact diatom coastal zone primary production here.

Primary production of diatoms is dependent upon DSi loading; shifting DIN and DIP loads over time, with respect to DSi, may shift coastal zone primary production from diatoms to non-siliceous algae (Billen and Garnier, 20007; Ludwig et al., 2009). DSi limitation can occur for diatoms in Mediterranean rivers, a persistent phenomenon between the 1970's and 1990's due to reductions in DIP loadings (Ludwig et al., 2009). The sandy beaches subject to wave-setup driven recirculation may transfer DIP to the coastal ocean as a remineralized nutrient product (Anschutz et al., 2009). However, DIP may be removed from groundwater and adsorbed onto the beach sediment in settings where sediment surfaces are coated with Fe-oxides (Charette and Sholkovitz, 2002). Future work studying coastal zone nutrient limitation should therefore carefully consider DSi loads driven by water recirculation, with respect to DIP and DIN loads.

5. Summary & Conclusions

In this study, we have quantified water recirculation through the permeable sediment of a coastal lagoon and along its adjacent sandy shoreline using Ra isotopes as tracers of water recirculation. We observed significant relationships between short-lived Ra isotopes and dissolved silica (DSi), which point toward a common source, the sediment. DSi enrichment from lithogenic particle (i.e. sediment) dissolution is supported by experimental dissolution rate calculations, which suggests that the DSi enrichments were not derived from diatom (i.e. biogenic) dissolution. The DSi flux from lagoon water recirculation is an order of magnitude greater than a local karstic groundwater spring and at least a factor of two greater than inputs from molecular diffusion. In comparison, the DSi flux from marine SGD along the 9.5 km sandy shoreline into the Mediterranean Sea, driven by wave-setup and water level differences between permeable sand barriers, is similar to the DSi flux from the nearby Têt River, the largest river in the region. Upscaling this flux to the permeable sandy shoreline of the Gulf of Lions results in a DSi flux that is one to two orders of magnitude lower than the Rhône River; however, the importance of recirculation-driven DSi inputs may be significant for Mediterranean shoreline segments that are not impacted by terrestrial (riverine and groundwater) DSi inputs. Despite these large recirculation-driven DSi fluxes, coastal-zone primary production is limited by inputs of DIN to the lagoon and DIP to the coastal Mediterranean Sea.

6. Acknowledgments

This study was funded by ANR-MED-SGD (ANR-15-CE01-0004; PI: Pieter van Beek). The postdoctoral fellowship of Joseph Tamborski and the PhD thesis of Simon Bejannin are supported by FEDER funded by Europe and Région Occitanie Pyrénées-Méditerranée (SELECT project). The fellowship of Céline Charbonnier is supported by ANR-MED-SGD. Jordi Garcia Orellana wants to thank the support of the Generalitat de Catalunya to MERS (2018 SGR-1588).

This work is contributing to the ICTA 'Unit of Excellence' (MinECo, MDM2015-0552). Thomas Stieglitz holds a chair at RAction of the French Agence National de Recherche ANR (ANR-14-ACHN-0007-01, project medLOC), and is supported by the Labex OT-Med (ANR-11-LABEX-0061) funded by the "Investissements d'Avenir" program through the AMIDEX project (ANR-11- IDEX-0001-02). Valentí Rodellas acknowledges financial support from the European Union's Horizon 2020 research and innovation programme under the Marie Skłodowska-Curie grant agreement No 748896. We thank Eric Martinez, Arnaud Catania, Germain Maldonado and Christophe Mariotti from R.V. NEREIS II. We thank Jean-François Ghiglione, Jocelyne Caparros, Audrey Gueneugues, Jean-Luc Seidel and Carolina Olid for help in sampling during the field trip in La Palme in June 2016. We are grateful to Kattalin Fortuné-Sans and Camille Pfleger (Parc Naturel Régional de la Narbonnaise en Méditerranée) and Laurence Fonbonne (Syndicat mixte RIVAGE Salses-Leucate).

7. References

Aminot A., Kérouel R. (2007) Dosage automatique des nutriments dans les eaux marines : méthodes en flux continu, Ifremer ed., 188 pp.

Anschutz P., Charbonnier C., Deborde J., Deirmendjian L., Poirier D., Mouret A., Buquet D., Lecroart P. (2016) Terrestrial groundwater and nutrient discharge along the 240-km-long Aquitanian coast. *Marine Chemistry* **185**: 38-47. doi: 10.1016/j.marchem.2016.04.002

Anschutz P., Deborde J. (2016) Spectrophotometric determination of phosphate in matrices from sequential leaching of sediments. *Limnology & Oceanography Methods* **14**: 245-256. doi:

Anschutz P., Smith T., Mouret A., Deborde J., Bujan S., Poirier D., Lecroart P. (2009) Tidal sands as biogeochemical reactors. *Estuarine, Coastal and Shelf Science* **84**: 84-90. doi: 10.1002/lom3.1008510.1016/j.ecss.2009.06.015

699 Beck A., Cochran J., Sanudo-Wilhelmy S. (2010) The distribution and speciation of dissolved trace
700 metals in a shallow subterranean estuary. *Marine Chemistry* **121(1-4)**: 145-156. doi:
701 10.1016/j.marchem.2010.04.003
702 Beck A., Rapaglia J., Cochran J., Bokuniewicz H. (2007) Radium mass-balance in Jamaica Bay,
703 NY: Evidence for a substantial flux of submarine groundwater. *Marine Chemistry* **106(3-4)**: 419-
704 441. doi: 10.1016/j.marchem.2007.03.008
705 Berner R.A. (1980) Early diagenesis: A theoretical approach. Princeton Univ. Press. 245p.
706 Bejannin S., van Beek P., Stieglitz T., Souhaut M., Tamborski J. (2017) Combining airborne
707 thermal infrared images and radium isotopes to study submarine groundwater discharge along
708 the French Mediterranean coastline. *Journal of Hydrology: Regional Studies* **13**: 72-90. doi:
709 10.1016/j.ejrh.2017.08.001
710 Billen G., Garnier J. (2007) River basin nutrient delivery to the coastal sea: Assessing its potential
711 to sustain new production of non-siliceous algae. *Marine Chemistry* **106**: 148-160. doi:
712 10.1016/j.marchem.2006.12.017
713 Blanc P., Lassin A., Piantone P., Azaroual M., Jacquemet N., Fabbri A., Gaucher E.C. (2012)
714 Thermoddem: A geochemical database focused on low temperature water/rock interactions and
715 waste materials. *Applied Geochemistry* **27**: 2107-2116. doi: 10.1016/j.apgeochem.2012.06.002
716 Boudreau B.P. (1996) The diffusive tortuosity of fine-grained unlithified sediments. *Geochemica et*
717 *Cosmochimica Acta* **60(16)**: 3139-3142. doi: 1016/0016-7037(96)00158-5
718 Burnett W., Aggarwal P., Aureli A., Bokuniewicz H., Cable J., Charette M., Kontar E., Krupa S.,
719 Kulkarni K., Loveless A., Moore W., Oberdorfer J., Oliveira J., Ozyurt N., Povinec P., Privitera
720 A., Rajar R., Ramassur R., Scholten J., Stieglitz T., Taniguchi M., Turner J. (2006) Quantifying
721 submarine groundwater discharge in the coastal zone via multiple methods. *Science of the Total*
722 *Environment* **367(2-3)**: 498-543. doi: 10.1016/j.scitotenv.2006.05.009
723 Burnett W.C., Bokuniewicz H., Huettel M., Moore W.S., Taniguchi M. (2003) Groundwater and
724 pore water inputs to the coastal zone. *Biogeochemistry* **66**: 3-33. doi:
725 10.1023/B:BIOG.0000006066.21240.53
726 Cai P., Shi X., Moore W.S., Peng S., Wang G., Dai M. (2014) ^{224}Ra:^{228}Th disequilibrium in coastal
727 sediments: Implications for solute transfer across the sediment-water interface. *Geochimica et*
728 *Cosmochimica Acta* **125**: 68-84. doi: 10.1016/j.gca.2013.09.029

729 Charette M.A., Sholkovitz E.R. (2002) Oxidative precipitation of groundwater-derived ferrous iron
730 in the subterranean estuary of a coastal bay. *Geophysical Research Letters* **29(10)**: 1444. doi:
731 10.1029/2001GL014512
732 Cook P.G., Rodellas V., Andrisoa A., Stieglitz T.C. (2018) Exchange across the sediment-water
733 interface quantified from porewater radon profiles. *Journal of Hydrology* **559**: 873-883. doi:
734 10.1016/j.hydrol.2018.02.070
735 Cyronak T., Santos I.R., Erler D.V., Maher D.T., Eyre B.D. (2014) Drivers of pCO_2 variability in
736 two contrasting coral reef lagoons: The influence of submarine groundwater discharge. *Global*
737 *Biogeochemical Cycles* **28(4)**: 398-414. doi: 10.1002/2013GB004598
738 Colbert S.L., Hammond D.E. (2007) Temporal and spatial variability of radium in the coastal ocean
739 and its impact on computation of nearshore cross-shelf mixing rates. *Continental Shelf Research*
740 **27(10-11)**: 1477-1500. doi: 10.1016/j.csr.2007.01.003
741 Durrieu de Madron X. et al. (2011) Marine ecosystems' responses to climatic and anthropogenic
742 forcings in the Mediterranean. *Progress in Oceanography* **91(2)**: 97-166. doi:
743 10.1016/j.pocean.2011.02.003
744 Ehlert C., Reckhardt A., Greskowiak J., Liguori B.T.P., Boning P., Paffrath R., Brumsack H.J.,
745 Pahnke K. (2016) Transformation of silicon in a sandy beach ecosystem: Insights from stable
746 silicon isotopes from fresh and saline groundwaters. *Chemical Geology* **440**: 207-218. doi:
747 10.1016/j.chemgeo.2016.07.015
748 El-Gamal A., Peterson R., Burnett W. (2012) Detecting Freshwater Inputs via Groundwater
749 Discharge to Marina Lagoon, Mediterranean Coast, Egypt. *Estuaries and Coasts* **35(6)**: 1486-
750 1499. doi: 10.1007/s12237-012-9539-2
751 Fleury P., Bakalowicz M., de Marsily G. (2007). Submarine springs and coastal karst aquifers: a
752 review. *J. Hydrol.* **339**, 79-92. doi: 10.1016/j.jhydrol.2007.03.009
753 Garcia-Orellana J., Rodellas V., Casacuberta N., Lopez-Castillo E., Vilarrasa M., Moreno V.,
754 Garcia-Solsona E., Masque P. (2013) Submarine groundwater discharge: Natural radioactivity
755 accumulation in a wetland ecosystem. *Marine Chemistry* **156**: 61-72. doi:
756 10.1016/j.marchem.2013.02.004
757 Garcia-Solsona E., Garcia-Orellana J., Masque P., Dulaiova H. (2008a) Uncertainties associated
758 with Ra-223 and Ra-224 measurements in water via a Delayed Coincidence Counter (RaDeCC).
759 *Marine Chemistry* **109(3-4)**: 198-219. doi: 10.1016/j.marchem.2007.11.006

760 Garcia-Solsona E., Masque P., Garcia-Orellana J., Rapaglia J., Beck A.J., Cochran J.K.,
761 Bokuniewicz H.J., Zaggia L., Collavini F. (2008b) Estimating submarine groundwater discharge
762 around Isola La Cura, northern Venice Lagoon (Italy), by using the radium quartet. *Marine*
763 *Chemistry* **109(3-4)**. doi: 10.1016/j.marchem.2008.02.007
764 Garcia-Solsona E., Garcia-Orellana J., Masque P., Garces E., Radakovitch O., Mayer A., Estrade S.,
765 Basterretxea G. (2010a) An assessment of karstic submarine groundwater and associated nutrient
766 discharge to a Mediterranean coastal area (Balearic Islands, Spain) using radium isotopes.
767 *Biogeochemistry* **97(2-3)**: 211-229. doi: 10.1007/s10533-009-9368-y
768 Garcia-Solsona E., Garcia-Orellana J., Masque P., Rodellas V., Mejias M., Ballesteros B.,
769 Dominguez J. (2010b) Groundwater and nutrient discharge through karstic coastal springs
770 (Castello, Spain). *Biogeosciences* **7(9)**: 2625-2638. doi: 10.5194/bg-7-2625-2010
771 IFREMER (2003) Réseau de Suivi Lagunaire du Languedoc-Roussillon: 4 - Etang de La Palme.
772 Sète, France
773 Jeandel C., Oelkers E. (2015) The influence of terrigenous particulate material dissolution on ocean
774 chemistry and global element cycles. *Chemical Geology* **395**: 50-66. doi:
775 10.1016/j.chemgeo.2014.12.001
776 Justic D., Rabalais N., Turner R. (1995) Stoichiometric nutrient balance and origin of coastal
777 eutrophication. *Marine Pollution Bulletin* **30**: 41-46. doi: 10.1016/0025-326X(94)00105-I
778 Kim G., Ryu J.W., Yang H.S., Yun S.T. (2005) Submarine groundwater discharge (SGD) into the
779 Yellow Sea revealed by ^{228}Ra and ^{226}Ra isotopes: Implications for global silicate fluxes. *Earth*
780 *and Planetary Science Letters* **237**: 156-166. doi: 10.1016/j.epsl.2005.06.011
781 Krom M.D., Emeis K.C., Van Cappellen P. (2010) Why is the Eastern Mediterranean phosphorus
782 limited? *Progress in Oceanography* **85**: 236-244. doi: 10.1016/j.pocean.2010.03.003
783 Lee Y.W., Hwang D.W., Kim G., Lee W.C., Oh H.T. (2009) Nutrient inputs from submarine
784 groundwater discharge (SGD) in Masan Bay, an embayment surrounded by heavily
785 industrialized cities, Korea. *Science of the Total Environment* **407**: 3181-3188. doi:
786 10.1016/j.scitotenv.2008.04.013
787 Loucaide S., Van Cappellen P., Behrends T. (2008) Dissolution of biogenic silica from land to
788 ocean: Role of salinity and pH. *Limnology and Oceanography* **53**: 1614-1621. doi:
789 10.4319/lo.2008.53.4.1614

790 Ludwig W., Dumont E., Meybeck M., Heussner S. (2009) River discharges of water and nutreints
791 to the Mediterranean and Black Sea: Major drivers for ecosystem changes during past and future
792 decades? *Progress in Oceanography* **80**: 1999-217. doi: 10.1016/j.pocean.2009.02.001
793 Luek J.L., Beck, A.J. (2014) Radium budget of the York River estuary (VA, USA) dominated by
794 sumbarine groundwater dischage with a seasonally variable groundwater end-member. *Marine*
795 *Chemistry* **165**: 55-65. doi: 10.1016/j.marchem.2014.08.001
796 Michael H., Mulligan A., Harvey C. (2005) Seasonal oscillations in water exchange between
797 aquifers and the coastal ocean. *Nature* **436(7054)**: 1145-1148. doi: 10.1038/nature03935
798 Moore W.S. (1996) Large groundwater inputs to coastal waters revealed by Ra-226 enrichments.
799 *Nature* **380(6575)**: 612-614. doi: 10.1038/380612a0
800 Moore W.S. (1999) The subterranean estuary: a reaction zone of ground water and sea water.
801 *Marine Chemistry* **65(1-2)**: 111-125. doi: 10.1016/S0304-4203(99)00014-6
802 Moore W.S. (2000a) Determining coastal mixing rates using radium isotopes. *Continental Shelf*
803 *Research* **20(15)**: 1993-2007. doi: 10.1016/S0278-4343(00)00054-6
804 Moore W.S. (2000b) Ages of continental shelf waters determined from Ra-223 and Ra-224. *Journal*
805 *of Geophysical Research-Oceans* **105(C9)**: 22117-22122. doi: 10.1029/1999jc000289
806 Moore W.S. (2008) Fifteen years experience in measuring ^{224}Ra and ^{223}Ra by delayed-coincidence
807 counting. *Marine Chemistry* **109**: 188-197. doi: 10.1016/j.marchem.2007.06.015

808 Moore W.S., Arnold R. (1996) Measurement of Ra-223 and Ra-224 in coastal waters using a
809 delayed coincidence counter. *Journal of Geophysical Research-Oceans* **101(C1)**: 1321-1329.
810 doi: 10.1029/95JC03139

811 Moore W.S. (2003) Sources and fluxes of submarine groundwater discharge delineated by radium
812 isotopes. *Biogeochemistry* **66**: 75-93. doi: 10.1023/B:BIOG.0000006065.77764.a0
813 Moore W.S., Blanton J.O., Joye S.B. (2006) Estimates of flushing times, submarine groundwater
814 discharge, and nutrient fluxes to Okatee Estuary, South Carolina. *Journal of Geophysical*
815 *Research* **111**: C09006. doi: 10.1029/2005JC003041
816 Morin G., Vigier N., Verney-Carron A. (2015) Enhanced dissolution of basaltic glass in brackish
817 waters: Impact on biogeochemical cycles. *Earth Planet. Sci. Lett.* **417**: 1-8. doi:
818 10.1016/j.epsl.2015.02.005

819 Null K.A., Knee K.L., Crook E.D., de Sieyes N.R., Rebolledo-Vieyra M., Hernandez-Terrones L.,
820 Paytan A. (2014) Composition and fluxes of submarine groundwater along the Caribbean coast
821 of the Yucatan Peninsula. *Continental Shelf Research* **77**: 38-50. doi: 10.1016/j.csr.2014.01.011
822 Parkhurst D.L., Appelo C.A.J. (2013) Description of input and examples for PHREEQC version 3:
823 a computer program for speciation, batch-reaction, one-dimensional transport, and inverse
824 geochemical calculations. In, Techniques and Methods 6-A43, Section A: Groundwater, U.S.
825 Geological Survey
826 Rodellas V., Garcia-Orellana J., Masque P., Feldman M., Weinstein Y. (2015) Submarine
827 groundwater discharge as a major source of nutrients to the Mediterranean Sea. *Proceedings of*
828 *the National Academy of Sciences of the United States of America* **112(13)**: 3926-3930. doi:
829 10.1073/pnas.1419049112
830 Rodellas V., Garcia-Orellana J., Trezzi G., Masque P., Stieglitz T.C., Bokuniewicz H., Cochran
831 J.K., Berdalet E. (2017) Using the radium quartet to quantify submarine groundwater discharge
832 and porewater exchange. *Geochimica et Cosmochimica Acta* **196**: 58-73. doi:
833 10.1016/j.gca.2016.09.016
834 Rodellas V., Stieglitz T.C., Andrisoa A., Cook P.G., Raimbault P., Tamborski J.J., van Beek P.,
835 Radakovitch O. (2018) Groundwater-driven nutrient inputs to coastal lagoons: The relevance of
836 lagoon water recirculation as a conveyor of dissolved nutrients. *Science of the Total Environment*
837 **642**: 764-780. doi: 10.1016/j.scitotenv.2018.06.095
838 Sadaoui M., Ludwig W., Bourrin F., Raimbault P. (2016) Controls, budgets and variability of
839 riverine sediment fluxes to the Gulf of Lions (NW Mediterranean Sea). *Journal of Hydrology*
840 **540**: 1002-1015. doi: 10.1016/j.hydrol.2016.07.012
841 Santos I., Eyre B., Huettel M. (2012) The driving forces of porewater and groundwater flow in
842 permeable coastal sediments: A review. *Estuarine Coastal and Shelf Science* **98**: 1-15. doi:
843 10.1016/j.ecss.2011.10.024
844 Schroeder K., Gasparini G.P., Borghini M., Cerrati G., Delfanti R. (2010) Biogeochemical tracers
845 and fluxes in the Western Mediterranean Sea, spring 2005. *Journal of Marine Systems* **80**: 8-24.
846 doi: 10.1016/j.marsys.2009.08.002
847 Schulz H.D., Zabel M. (2006) *Marine Geochemistry*. 2nd edition. Springer, Berlin Heidelberg New
848 York.

849 Slomp C., Van Cappellen P. (2004) Nutrient inputs to the coastal ocean through submarine
850 groundwater discharge: controls and potential impact. *Journal of Hydrology* **295(1-4)**: 64-86.
851 doi: 10.1016/j.jhydrol.2004.02.018
852 Stieglitz T., van Beek P., Souhaut M., Cook P. (2013) Karstic groundwater discharge and seawater
853 recirculation through sediments in shallow coastal Mediterranean lagoons, determined from
854 water, salt and radon budgets. *Marine Chemistry* **156**: 73-84. doi:
855 10.1016/j.marchem.2013.05.005
856 Sugimoto R., Kitagawa K., Nishi S., Honda H., Yamada M., Kobayashi S., Shoji J., Ohsawa S.,
857 Taniguchi M., Tominaga O. (2017) Phytoplankton primary productivity around submarine
858 groundwater discharge in nearshore coasts. *Marine Ecology Progress Series* **563**: 25-33. doi:
859 10.3354/meps11980
860 Sun Y., Torgersen T. (1998) The effects of water content and Mn-fiber surface conditions on ^{224}Ra
861 measurement by ^{220}Rn emanation. *Marine Chemistry* **62(3-4)**: 299-306. doi: 10.1016/S0304-
862 4203(98)00019-X
863 Swarzenski P. (2007) U/Th series radionuclides as coastal groundwater tracers. *Chemical Reviews*
864 **107(2)**: 663-674. doi: 10.1021/cr0503761
865 Techer I., Advocat T., Lancelot J., Liotard J. (2001) Dissolution kinetics of basaltic glasses: Control
866 by solution chemistry and protective effect of the alteration film. *Chem. Geol.* **176**: 235-263. doi:
867 10.1016/S0009-2541(00)00400-9
868 Tovar-Sánchez A., Basterretxea G., Rodellas V., Sánchez-Quiles D., Gacria-Orellana J., Masqué P.,
869 Jordi A., Lopez J.M., Garcia-Solsona E. (2014). Contribution of groundwater discharge to the
870 coastal dissolved nutrients and trace metal concentrations in Majorca Island: Karstic vs detrital
871 systems. *Environmental Science & Technology* **48**: 11819-11827. doi: 10.1021/es502958t
872 Tréguer P., De La Rocha C. (2013) The world ocean silica cycle. *Ann. Rev. Mar. Sci.* **5**: 477-501.
873 doi: 10.1146/annurev-marine-121211-172346
874 Trezzi G., Garcia-Orellana J., Rodellas V., Santos-Echeandia J., Tovar-Sánchez A., Garcia-Solsona
875 E., Masqué P. (2016) Submarine groundwater discharge: A significant source of dissolved trace
876 metals to the North Western Mediterranean Sea. *Marine Chemistry* **186**: 90–100.
877 doi:10.1016/j.marchem.2016.08.004

878 Ullman W.J., Chang B., Miller D.C., Madsen J.A. (2003) Groundwater mixing, nutrient diagenesis,
879 and discharges across a sandy beachface, Cape Henlopen, Delaware (USA). *Estuarine, Coastal*
880 *and Shelf Science* **57**: 539-552. doi: 10.1016/S0272-7714(02)00398-0
881 Urquidi-Gaume M., Santos I.R., Lechuga-Deveze C. (2016) Submarine groundwater discharge as a
882 source of dissolved nutrients to an arid coastal embayment (La Paz, Mexico). *Environmental*
883 *Earth Sciences* **75**:154. doi: 10.1007/s12665-015-4891-8
884 Webster I.T., Hancock G.J., Murray A.S. (1995) Modelling the effect of salinity on radium
885 desorption from sediments. *Geochemica et Cosmochimica Acta* **59(12)**: 2469-2476. doi:
886 10.1016/0016-7037(95)00141-7
887 Weinstein Y., Yechieli Y., Shalem Y., Burnett W.C., Swarzenski P.W., Herut B. (2011) What is the
888 role of fresh groundwater and recirculated seawater in conveying nutrients to the coastal ocean?
889 *Environmental Science and Technology* **45**: 5195-5200. doi: 10.1021/es104394r
890 Welti N., Gale D., Hayes M., Kumar A., Gasparon M., Gibbes B., Lockington D. (2015) Intertidal
891 diatom communities reflect patchiness in groundwater discharge. *Estuarine, Coastal and Shelf*
892 *Science* **163(B)**: 116-124. doi: 10.1016/j.ecss.2015.06.006
893
894
895
896
897
898
899
900
901
902
903
904
905
906

Tables

Table 1. Mean (± STD) lagoon water (northern, intermediate and southern), karstic groundwater spring and lagoon pore water salinity, ^{223}Ra, $^{224}Ra_{ex}$, ^{228}Ra and DSi during June 2016. Shallow PW = shallow lagoon pore water samples. DSi concentrations are from <10 cm depth, used in the flux calculation (June 2016, May 2017 and September 2017). Shallow pore water DSi concentrations are corrected for overlying lagoon water DSi. Shallow Ra activities are from 20 – 40 cm depth. Deep PW = lagoon pore water samples between 50 – 140 cm depth from the drive-point piezometers; DSi concentrations are for 50 cm depth only (June 2016).

Endmember	Salinity	^{223}Ra	$^{224}Ra_{ex}$	^{228}Ra	DSi	n
		dpm $100L^{-1}$	dpm $100L^{-1}$	dpm $100L^{-1}$	µM	
Northern	33 ± 5	6 ± 2	180 ± 120	270 ± 70	15 ± 21	Ra=27; DSi=24
Intermediate	40 ± 2	9 ± 4	140 ± 30	280 ± 40	4 ± 4	Ra=15; DSi=15
Southern	42 ± 3	12 ± 4	230 ± 80	190 ± 90	9 ± 7	Ra=15; DSi=14
Spring	8.4 ± 0.7	11 ± 3	710 ± 80	450 ± 30	114.0 ± 0.2	Ra=4; DSi=3
Shallow PW	38 ± 8	70 ± 49	1,060 ± 740	500 ± 450	32 ± 14	Ra=5; DSi=17
Deep PW	59 ± 16	400 ± 270	5,500 ± 3,900	2,800 ± 1,900	129 ± 23	Ra=7; DSi=3

Table 2. Summary of lagoon water pH and relevant saturation state indices (± STD), determined using PHREEQC. Negative values indicate under-saturation conditions, positive values indicate saturation conditions.

	pH	Barite	Celestine	Quartz	Amorphous Silica	n
			log SI			
Northern	8.41 ± 0.23	0.09 ± 0.02	-0.84 ± 0.06	-1.3 ± 0.3	-2.3 ± 0.3	23
Intermediate	8.35 ± 0.03	0.12 ± 0.03	-0.76 ± 0.01	-1.6 ± 0.2	-2.6 ± 0.2	7
Southern	8.35 ± 0.15	-0.10 ± 0.20	-0.75 ± 0.03	-1.3 ± 0.3	-2.3 ± 0.3	11

Table 3. Diffusive DSi fluxes to La Palme lagoon (May and September 2017) at the sediment water interface, arranged by lagoon basin.

Basin	Surface area $*10^6$ m^2	Diffusive flux May mol d^{-1}	Diffusive flux Sept. mol d^{-1}
Northern	2.48	145 ± 176	817 ± 747
Intermediate	1.55	23 ± 20	48 ± 25
Southern	0.53	32 ± 23	106 ± 61
Total	4.56	201 ± 179	972 ± 750

Table 4. Summary of the terms used in the Ra mass balance. The groundwater spring inflow has an assumed uncertainty of 20%.

Term	Description	Value	Units
A	Lagoon Surface Area	4.56 ± 0.23	$*10^6$ m^2
V	Lagoon Volume	2.28 ± 0.11	$*10^6$ m^3
Q_{spring}	Groundwater Spring Inflow	0.025 ± 0.005	m^3 s^{-1}
C_{sed}	Suspended Solids	40 ± 10	mg L^{-1}
X_{desorp}	^{223}Ra available for desorption	0.008 ± 0.007	dpm g^{-1}
X_{desorp}	^{224}Ra available for desorption	0.24 ± 0.05	dpm g^{-1}
$J_{sediment}$	^{223}Ra diffusive flux from fine sediment	3.6 ± 1.4	dpm m^{-2} d^{-1}
$J_{sediment}$	^{224}Ra diffusive flux from fine sediment	75 ± 50	dpm m^{-2} d^{-1}
$J_{sediment}$	^{228}Ra diffusive flux from fine sediment	15 ± 8	dpm m^{-2} d^{-1}

Table 5. Summary of DSi fluxes to La Palme lagoon (June 2016) and the coastal Mediterranean Sea (November 2016). The marine SGD flux to the coastal Mediterranean Sea is for the 9.5 km long stretch of shoreline from the outlet of La Palme lagoon to Port-la-Nouvelle (Figure 1).

	DSi Flux
	* 10^3 mol d^{-1}
Lagoon	
Groundwater spring	0.25 ± 0.05
Water recirculation	1.93 ± 1.65
Molecular diffusion	0.97 ± 0.75
Mediterranean Sea	
Marine SGD	23 ± 13
Têt river	33 ± 24

Figures

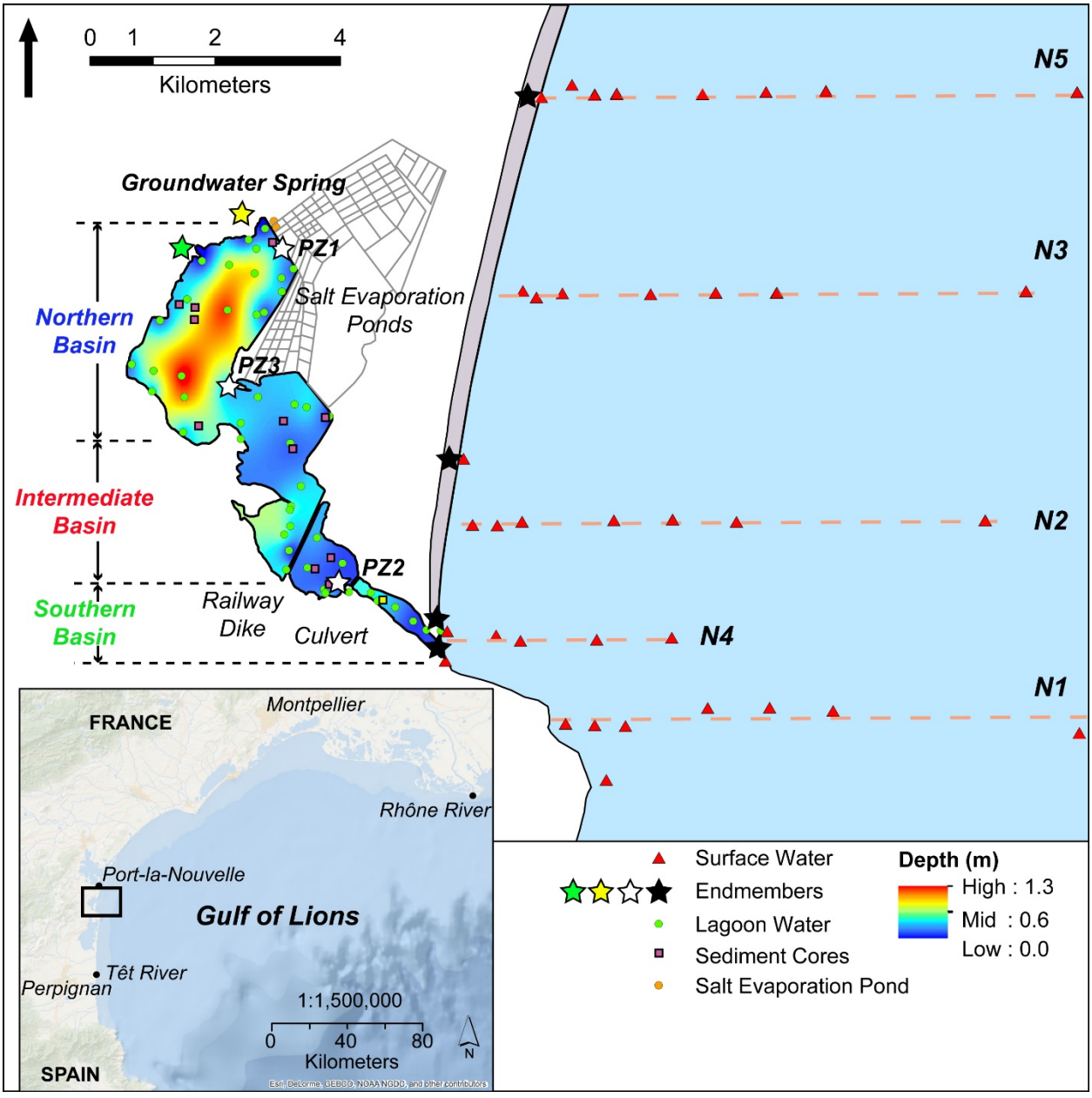

Figure 1. La Palme lagoon, located in southern France, adjacent to the Mediterranean Sea (inset; black square). Lagoon surface waters were collected during June 2016 (green circles), open surface water transects were collected during November 2016 (red triangles). Sediment cores (purple squares) were collected during May and September 2017. The sediment core for the DSi incubation experiment is indicated by a yellow square. The sediment core for the Ra diffusion experiment was collected next to PZ2. Lagoon water depth is specific to the June 2016 sampling period. Endmember samples are indicated by stars, including the sewage outlet (green), groundwater spring (yellow), lagoon pore waters (white) and beach pore waters (black). The gray shaded area indicates the sandy 9.5 km long shoreline (not to scale).

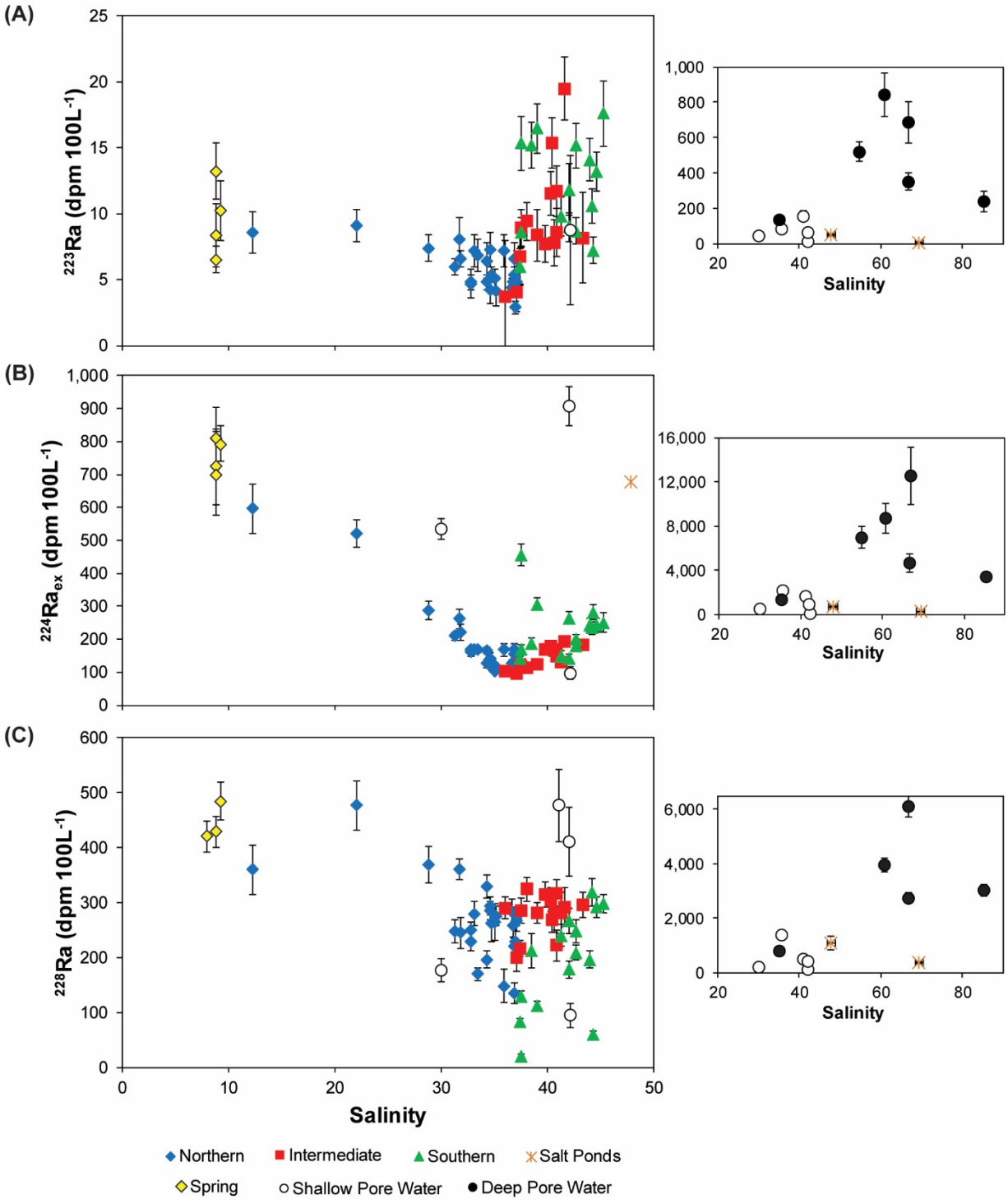

Figure 2. ^{223}Ra (A), ^{224}Ra$_{ex}$ (B) and ^{228}Ra (C) activity vs. salinity for La Palme lagoon surface waters and pore waters. Lagoon surface water samples are grouped by basin (northern, intermediate and southern). Pore water and salt pond samples are presented on the right-hand side for improved visualization. Note that most of these points are out of range on the left-hand panels. Shallow pore waters (20 – 40 cm) are indicated by hollow circles; deep pore waters (50 – 140 cm) are indicated by filled circles.

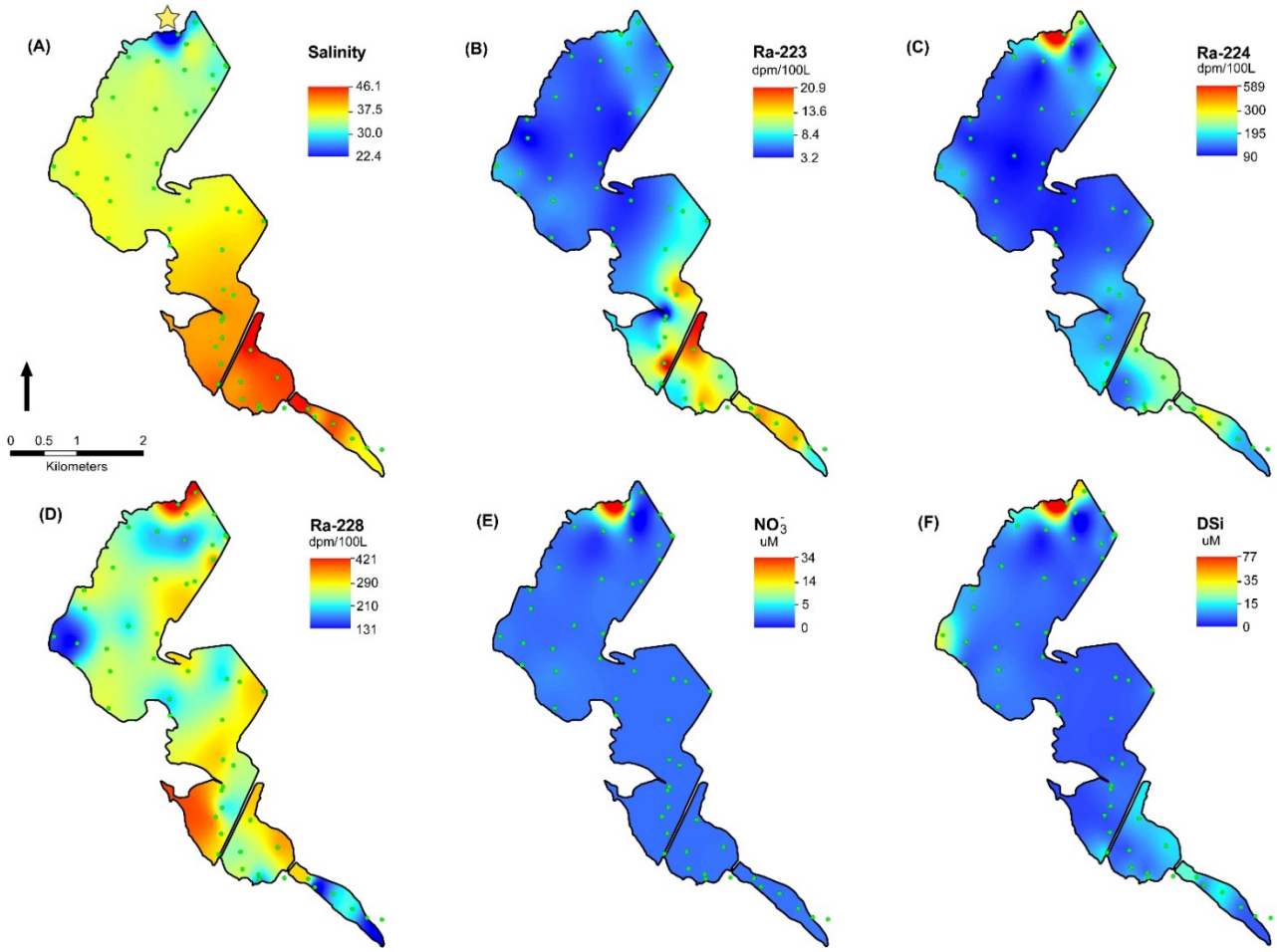

Figure 3. Interpolated surface water distributions of (A) salinity, (B) ^{223}Ra, (C) $^{224}Ra_{ex}$, (D) ^{228}Ra, (E) NO_3^- and (F) DSi in La Palme lagoon, during June 2016. The green dots represent the sampling locations. Note the interpolation color scale is not linear and differs between plots to improve visualization. The yellow star in (A) marks the location of the karstic groundwater spring.

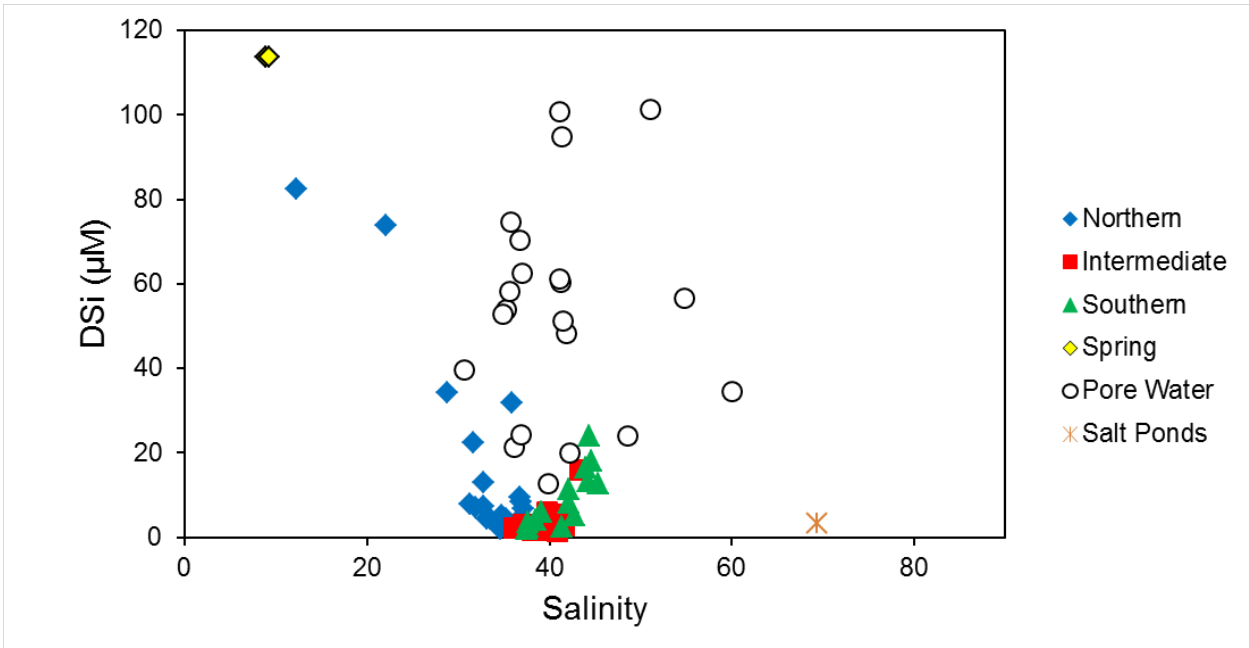

Figure 4. DSi vs. salinity for La Palme lagoon surface waters and pore waters collected during June 2016. Lagoon surface water samples are grouped by basin (northern, intermediate and southern). Pore water samples were taken from drive-point piezometers within the lagoon (Figure 1).

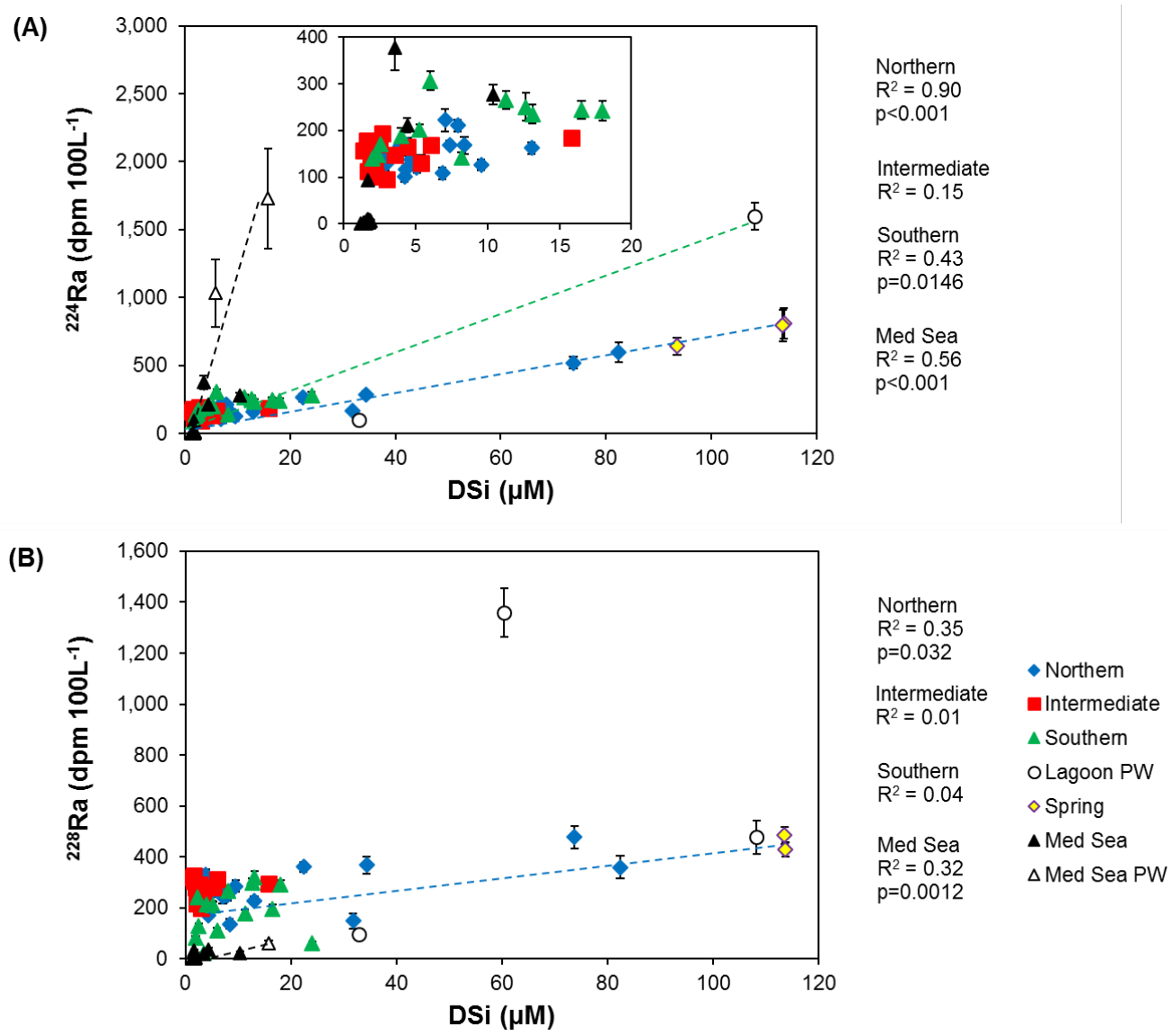

Figure 5. $^{224}Ra_{ex}$ (A) and ^{228}Ra (B) vs. DSi. Lagoon surface water samples are grouped by basin (northern, intermediate and southern). Lagoon pore waters (PW) are for shallow (20 – 40 cm) depths only, during June 2016. P-values and trend lines are only shown for statistically significant correlations.

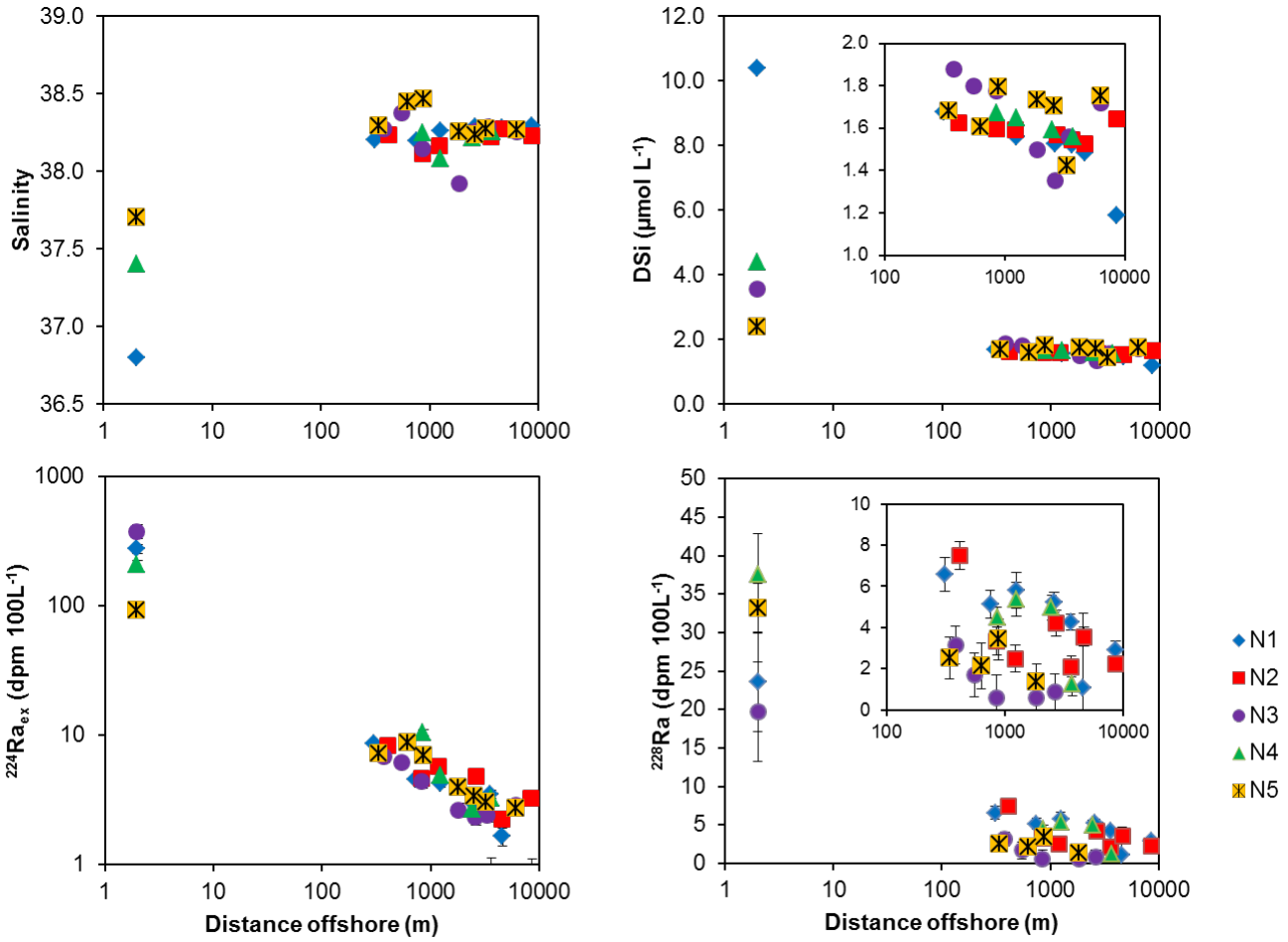

1077

1078 **Figure 6.** Surface water transects of salinity, DSi, (log) $^{224}Ra_{ex}$ and ^{228}Ra off the coast of La
1079 Palme lagoon into the coastal Mediterranean Sea, during November 2016.

1080

1081

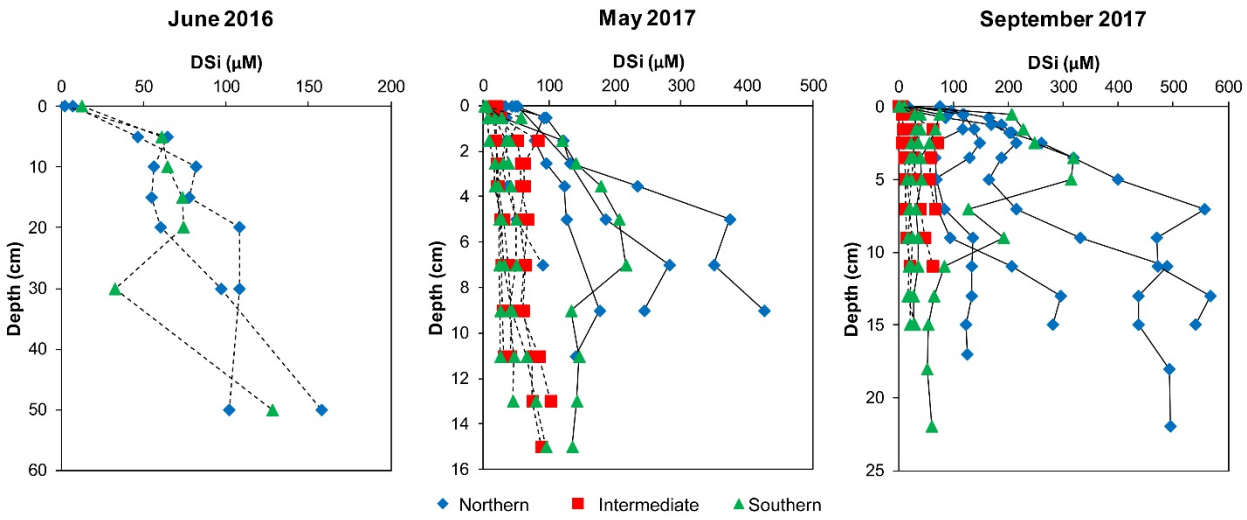

Figure 7. DSi concentration profiles in sediment cores collected in La Palme lagoon during June 2016, May 2017 and September 2017, grouped by lagoon basin (northern, intermediate and southern). Cores collected in permeable, sandy sediments are depicted by a dashed-line (mean down-core porosity ≤ 0.5); cores collected in impermeable, muddy sediments are depicted by a solid-line (mean down-core porosity > 0.5). Note the x- and y-axes differ between plots. June 2016 pore waters were taken by drive-point piezometer; May 2017 and September 2017 pore waters were extracted from sediment cores. Note that there is no sample for the intermediate basin during June 2016.

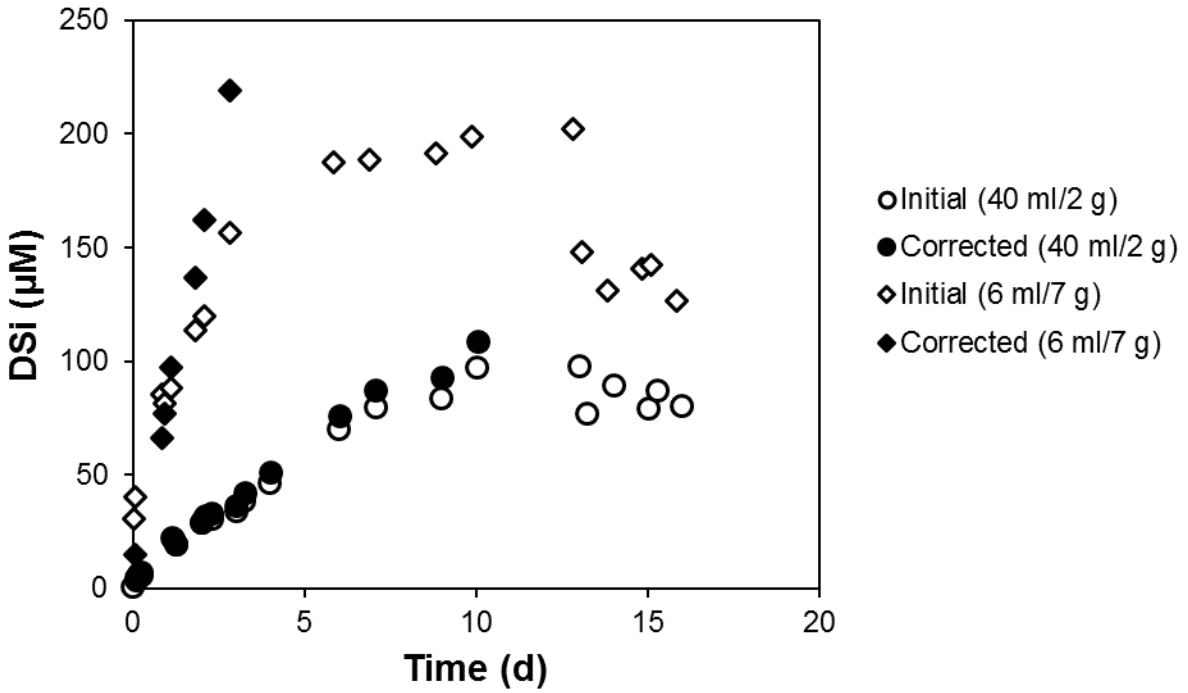

1100

1101 **Figure 8**. Evolution of DSi concentration during experimental incubations of La Palme lagoon
1102 sandy sediments for a water/rock ratio = 40 mL/2 g (circles) and a water/rock ratio = 6 mL/7 g
1103 (diamonds). Hollow symbols represent the measured DSi concentration; filled symbols represent
1104 the DSi concentration after correcting for sea water addition after water sampling.

1105

1106

1107

1108

1109

1110

1111

1112

1113

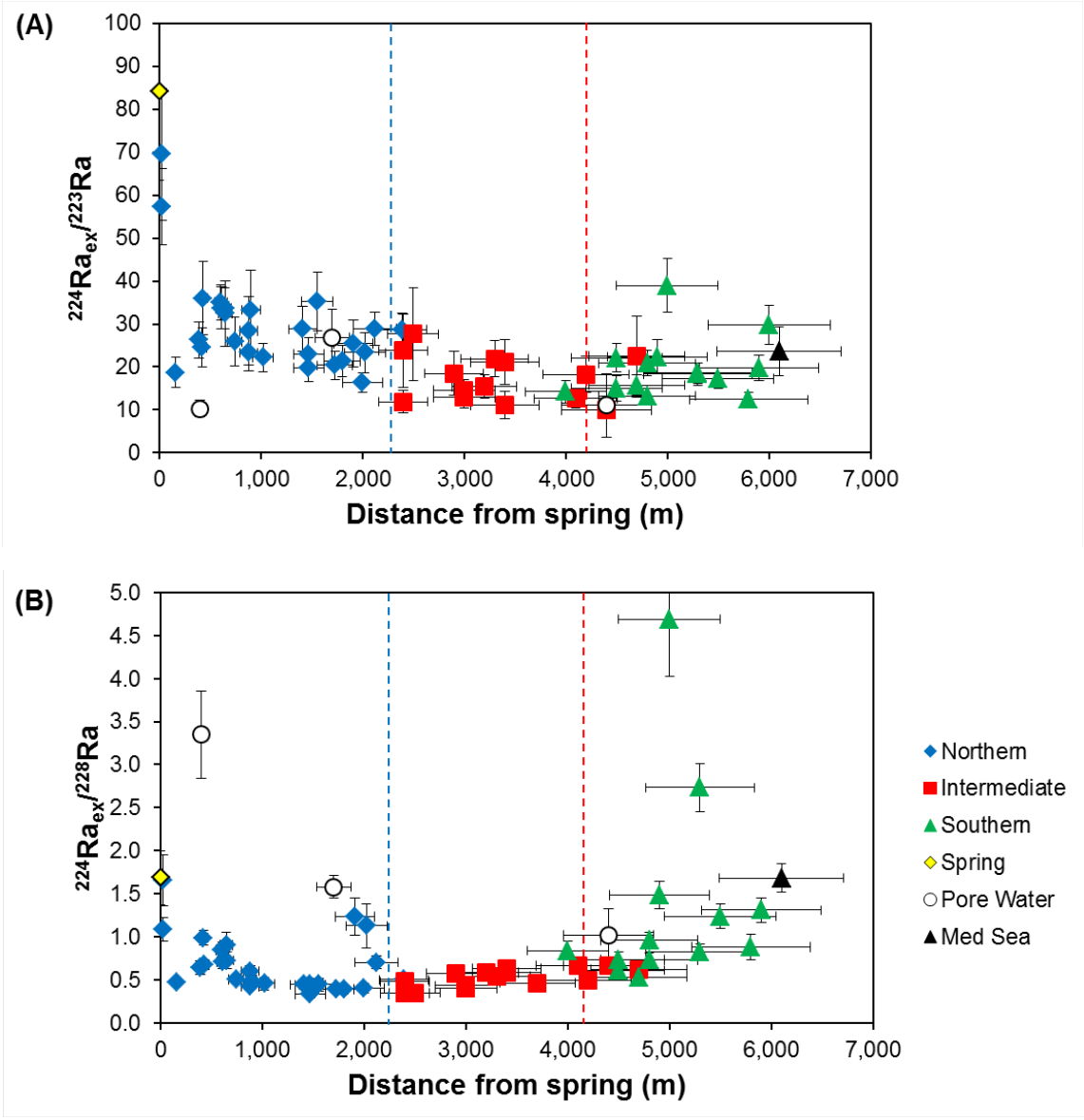

Figure 9. Lagoon surface water $^{224}Ra_{ex}/^{223}Ra$ (A) and $^{224}Ra_{ex}/^{228}Ra$ (B) activity ratios as a function of distance from the groundwater spring, during June 2016. Distances were measured using high resolution visible light imagery in Google Earth and assume a 10% measurement uncertainty. Shallow pore water endmember activity ratios (20 – 40 cm depth) are indicated by hollow circles (June 2016). The approximate interface between the northern and intermediate basin is indicated by a blue dashed line, and between the intermediate and southern basin by a red dashed line.

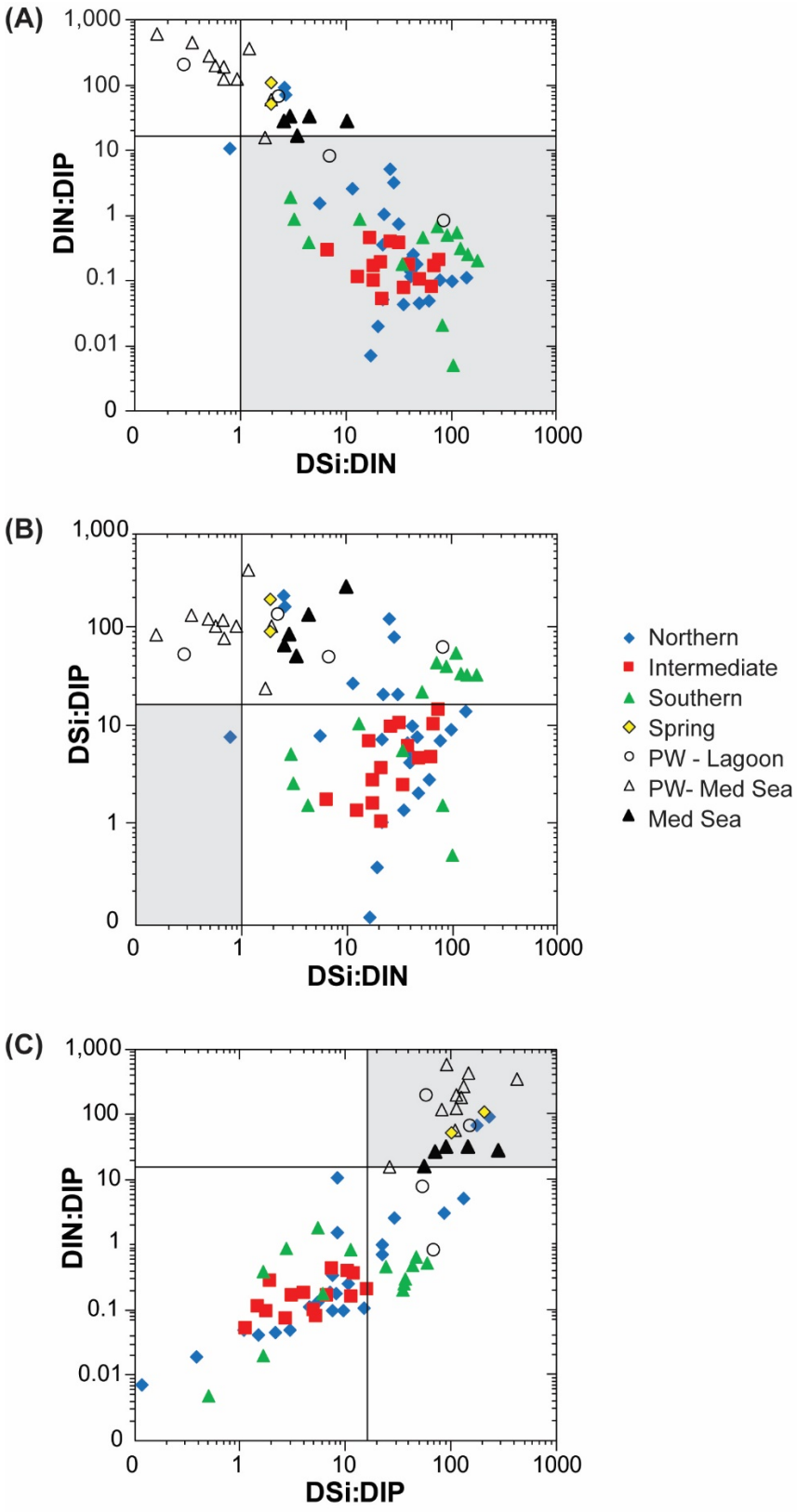

1124

1125 **Figure 10.** Stoichiometric ratios of DIN:DIP, DSi:DIN and DSi:DIP. Nutrient limitation is
1126 indicated by a shaded gray box for DIN (A), DSi (B) and DIP (C).